Analytical and Bioanalytical Chemistry. Accepted (uncorrected) version 24 November 2016

Biotransformation and detectability of the new psychoactive substances *N,N*-diallyltryptamine (DALT) derivatives 5-fluoro-DALT, 7-methyl-DALT, and 5,6-methylenedioxy-DALT in urine using GC-MS, LC-MS^n, and LC-HR-MS/MS

Julian A. Michely * Simon D. Brandt * Markus R. Meyer * Hans H. Maurer

---

J. A. Michely * M.R. Meyer * H. H. Maurer (corresponding author)

Department of Experimental and Clinical Toxicology, Institute of Experimental and Clinical Pharmacology and Toxicology, Saarland University, 66421 Homburg (Saar), Germany

e-mail: hans.maurer@uks.eu

Telephone: +49 – 6841 16 26050

Fax: +49 – 68941 16 26051

S. D. Brandt

School of Pharmacy and Biomolecular Sciences, Liverpool John Moores University, L3 3AF, Liverpool, United Kingdom

The Alexander Shulgin Research Institute, 1483 Shulgin Road, Lafayette, CA, 94549, USA

Abstract Derivatives of *N,N*-diallyltryptamine (DALT) can be classified as new psychoactive substances. Biotransformation and detectability of 5-fluoro-DALT (5-F-DALT), 7-methyl-DALT (7-Me-DALT), and 5,6-methylenedioxy-DALT (5,6-MD-DALT) are described here. Their metabolites detected in rat urine and pooled human liver microsomes were identified by liquid chromatography (LC)-high resolution (HR)-tandem mass spectrometry (MS/MS). In addition, the human cytochrome-P450 (CYP) isoenzymes involved in the main metabolic steps were identified and detectability tested in urine by the authors' urine screening approaches using GC-MS, LC-MS^n, or LC-HR-MS/MS. Aromatic and aliphatic hydroxylations, *N*-dealkylation, *N*-oxidation, and combinations could be proposed for all compounds as main pathways. Carboxylation after initial hydroxylation of the methyl group could also be detected for 7-Me-DALT and *O*-demethylenation was observed for 5,6-MD-DALT. All phase I metabolites were extensively glucuronidated or sulfated. Initial phase I reactions were catalyzed by CYP1A2, CYP2B6, CYP2C9, CYP2C19, CYP2D6, CYP3A4, and CYP3A5. Rat urine samples were analyzed following two different low dose administrations. GC-MS was not able to monitor consumption reliably, but all three drugs are predicted to be detectable in cases of overdose. The LC-MS^n and LC-HR-MS/MS approaches were suitable for detect an intake of all three compounds mainly via their metabolites. However, after the lowest dose, a reliable monitoring could only be achieved for 5-F-DALT via LC-MS^n and LC-HR-MS/MS and for 7-Me-DALT via LC-HR-MS/MS. The most abundant targets in both LC-MS screenings were one of two hydroxy-aryl metabolites and both corresponding glucuronides for 5-F-DALT, one *N*-deallyl hydroxy-aryl, the carboxy, and one dihydroxy-aryl metabolite for 7-Me-DALT, and the demethylenyl metabolite, its oxo metabolite, and glucuronide for 5,6-MD-DALT.

Keywords tryptamine derivatives; 5-F-DALT; 7-Me-DALT; 5,6-MD-DALT; metabolism; screening

Introduction

New psychoactive substances (NPS) represent an emerging issue worldwide. During the last years the number of reported NPS raised continuously [1-4]. According to the World Drug Report 2016 [4], synthetic tryptamines are still among the most commonly reported NPS besides synthetic cannabinoids, phenethylamines, synthetic cathinones, and piperazines. Both classic tryptamine psychedelics such as *N*,*N*-dimethyltryptamine (DMT) but also synthetic tryptamine-based "research chemicals" have been popular. [5, 6]. *N,N*-Diallyltryptamine (DALT) derivatives represent an important group with 5-methoxy-DALT (5-MeO-DALT) being the most often reported example [7-9]. As such drugs may become controlled the creation of new substances with similar chemical structures and effects is aimed at circumventing legislative restrictions [5], which leads to significant challenges for drug testing laboratories in the attempt to be kept up-to-date with analytical methods and reference data [10, 11]. One prerequisite is the knowledge of the NPS metabolism particularly for urine drug testing. Such data can only be generated if reference standards are available. One way to get them is to wait until their appearance on the drugs of abuse market or to synthesize potential derivatives in anticipation of future occurrences on the market.

In a previous study, DALT and 5-MeO-DALT were investigated in detail concerning metabolism and urinalysis [9]. The present study describes the biotransformation and detectability of three ring substituted DALT derivatives 5-fluoro-DALT (5-F-DALT), 7-methyl-DALT (7-Me-DALT), and 5,6-methylenedioxy-DALT (5,6-MD-DALT), which were synthesized in advance of potential distribution as NPS [12]. As Cozzi and Daley [13] described pharmacological potency for 5-substitued DALTs and Wagmann et al. the inhibition of the monoamine oxidase A (publication in preparation) it can be assumed that such compounds will appear once on the drugs of abuse market. So far, only spectroscopic data [14] and an LC-MS^n approach for qualitative and quantitative of tryptamines in plasma and urine covering only the parent drugs [15] were published. In this investigation, it was aimed to i) identify the phase I and II metabolites in rat urine, ii)

confirm the phase I metabolites in pooled human liver microsomes (pHLM) by liquid chromatography (LC)-high resolution (HR)-MS/MS, iii) identify the human cytochrome-P450 (CYP) isoenzymes involved in the main metabolic steps, and iv) to test the detectability in urine by the authors' urine screening approaches (SUSA) using GC-MS [16], LC-MS^n [17], or LC-HR-MS/MS [18], respectively. With the help of the presented data and procedures, these compounds should be detected in potential clinical or forensic cases.

Experimental

Chemicals and reagents

5-F-DALT, 7-Me-DALT, 5,6-MD-DALT, and DALT-d_4 were synthesized as published previously [12], isocitrate and isocitrate dehydrogenase were purchased from Sigma (Taufkirchen, Germany), $NADP^+$ from Biomol (Hamburg, Germany), acetonitrile (LC-MS grade), ammonium formate (analytical grade), formic acid (LC-MS grade), methanol (LC-MS grade), and all other chemicals and biochemicals from VWR (Darmstadt, Germany). The baculovirus-infected insect cell microsomes (Supersomes) containing 1 nmol/mL of human cDNA-expressed CYP1A2, CYP2A6, CYP2B6, CYP2C8, CYP2C9, CYP2C19, CYP2D6, CYP2E1 (2 nmol/mL), CYP3A4, or CYP3A5 (2 nmol/mL), and pooled human liver microsomes (pHLM, 20 mg microsomal protein/mL, 400 pmol total CYP/mg protein) were obtained from BD Biosciences (Heidelberg, Germany). After delivery, the microsomes were thawed at 37 °C, divided into aliquots, snap-frozen in liquid nitrogen, and stored at -80 °C until use.

Urine samples

Investigations were performed as usual [9] with rat urine samples taken from male Wistar rats (Charles River, Sulzfeld, Germany) for toxicological diagnostic reasons. The test drugs were administered once in an aqueous suspension by gastric intubation in a single 20 mg/kg body mass (BM) dose for the identification of the metabolites and once in a single 1 or 0.1 mg/kg BM dose for toxicological analysis according to the German animal protection act. The rats were housed in metabolism cages for 24 h, having water ad libitum. Urine was collected separately from feces over a 24-h period. Blank urine samples were collected before drug administration to confirm the absence of interfering compounds. The samples were directly analyzed and then stored at -20 °C.

Sample preparation for identification of phase I and II metabolites by LC-HR-MS/MS

As described previously [9, 19], 500 µL of acetonitrile was added to 100 µL of urine. The mixture was shaken on a rotary shaker for 2 min. After centrifugation for 2 min at 10,000×*g*, 500 µL was transferred into a glass vial and evaporated to dryness under a gentle stream of nitrogen at 70 °C. The residue was dissolved in 50 µL of methanol. A 10-µL aliquot of each extract was then injected onto the LC-HR-MS/MS system.

Microsomal incubations for pHLM and initial CYP activity screening studies

Conditions for performing the microsomal incubations were published previously [9, 20]. Briefly, compounds (50 µmol/L each) were incubated with the CYP isoenzymes (50 pmol/mL, each) CYP1A2, CYP2A6, CYP2B6, CYP2C8, CYP2C9, CYP2C19, CYP2D6, CYP2E1, CYP3A4, CYP3A5, or pHLM (1 mg protein/mL) for 30 min. Reactions were initiated by addition of the substrate and stopped with 50 µL of ice-cold acetonitrile containing DALT-d_4 (1 mg/L) as internal standard. The solution was centrifuged for 2 min at 10,000×*g*, 50 µL of the supernatant phase were transferred to a glass vial and a 10-µL aliquot injected onto the LC-HR-MS/MS system.

LC-HR-MS/MS apparatus for identification of metabolites in urine and microsomal incubations

According to published procedures [9, 18], the extracts were analyzed using a Accela LC system consisting of an HTC PAL autosampler, a degasser, two 1250 quaternary pumps, an Aria Transcend TLX-I HTLC system, and a valve interface module with built-in switching valves, all controlled by the Aria software version 1.6.3, coupled to a Q-Exactive system equipped with a heated electrospray ionization (HESI)-II source and Xcalibur 2.2 SP1.48 software (all of ThermoFisher, Dreieich, Germany). Mass calibration was done according to the manufacturer's recommendations every 72 h using external mass calibration. The LC and MS conditions were according to Helfer et al. [18] and set as follows: a ThermoFisher Accucore PhenylHexyl column (100 mm × 2.1 mm I.D., 2.6 µm), guarded by an UHP filter cart (0.5 µm). Chromatography was performed at 35 °C maintained by an analytical column heater (HotDog 5090, Prolab, Reinach, Switzerland). The mobile phases consisted of 2 mM aqueous ammonium formate plus 0.1% formic acid (pH 3, eluent A) and 2 mM aqueous ammonium formate with acetonitrile:methanol (1:1, *v/v*; 1% water) plus 0.1% formic acid (eluent B). The flow rate was set to 0.5 mL/min for 10 min and 0.8 mL/min from 10-13.5 min. The gradient was programmed as follows: 0-1 min 99% A, 1-10 min to 1% A, 10-11.5 min hold 1% A, 11.5 - 13.5 min hold 99% A. The HESI-II source conditions were as follows: heater temperature, 320 °C; sheath gas, 60 arbitrary units (AU); auxiliary gas, 10 AU; spray voltage, 3.00 kV; capillary temperature, 320 °C; and S-lens RF level, 60.0. Mass spectrometry was performed in positive ionization mode using full scan mode and a subsequent data-dependent acquisition (DDA) mode. The settings for the full scan mode were as follows: scan range, *m/z* 130-1000; resolution, 35,000; microscans, 1; automatic gain control (AGC) target, 1e6; and maximum injection time (IT), 120 ms. The settings for the DDA mode were as follows: resolution, 17,500; microscans, 1; AGC target, 2e5; maximum IT, 250 ms; loop count, 5; isolation window,

m/z 1.0; high collision dissociation (HCD) cell stepped normalized collision energy (NCE), 17.5, 35, and 52.5%; spectrum data type, profile; intensity threshold, 4.0e3; dynamic exclusion, 8.0 s.

GC-MS SUSA

According to published procedures [9, 16], the urine sample (5 mL) was divided into two aliquots where one part was submitted to acid hydrolysis followed by extraction of the combined parts with a dichloromethane-isopropanol-ethyl acetate mixture. After evaporation, the residue was acetylated with an acetic anhydride-pyridine mixture under microwave irradiation, again evaporated and reconstituted in 100 µL of methanol. A 1-µL aliquot was injected onto the GC-MS system. This consisted of a Hewlett Packard (HP, Agilent, Waldbronn, Germany) 5890 Series II gas chromatograph combined with an HP 5972A MSD mass spectrometer and an HP MS ChemStation (DOS series) with HP G1034C software version C03.00. The GC conditions were as follows: splitless injection mode; column, ThermoFisher TG-1MS capillary (12 m x 0.2 mm I.D.); cross-linked methyl silicone, 330 nm film thickness; injection port temperature, 280 °C; carrier gas, helium; flow rate, 1 mL/min; column temperature, programmed from 100 to 310 °C at 30 °C/min; initial time, 2 min; final time, 5 min. The MS conditions were as follows: full scan mode, *m/z* 50-550; electron ionization (EI) mode, ionization energy, 70 eV; ion source temperature, 220 °C; and capillary direct interface, 280 °C.

The full scan data files were evaluated by the automated mass spectral deconvolution and identification system (AMDIS; http://chemdata.nist.gov/mass-spc/amdis/) in simple mode. The Maurer/Pfleger/Weber MPW_2016 library [21] was used as target library. The deconvolution parameter settings were as follows [22]: width, 32; adjacent peak subtraction, 2; resolution, high; sensitivity, very high; shape requirements, low; minimum match factor, 50.

LC-MS^n SUSA

The workup was identical to the procedure described above for identification of the metabolites. Analysis was performed using a LXQ linear ion trap MS equipped with an HESI-II source and coupled to an Accela LC system (all from ThermoFisher). The LC and the MS settings were described elsewhere [9, 19]. Briefly, DDA was conducted on precursor ions selected from MS^1: MS^1 was performed in the full scan mode (*m/z* 100-800) and MS^2 and MS^3 were performed in the DDA mode. ThermoFisher Xcalibur 2.2 SP1.48 software was used for data acquisition, NIST MS Search 2.0 (National Institute of Standards and Technology, Gaithersburg, MD, USA) for library generation, ThermoFisher ToxID 2.1.1 for automatic target screening in the MS^2 screening mode. The settings were as follows: retention time (RT) window, 20 min; RT, 0.1 min; signal threshold, 100; search index, 600; and reverse search index, 700. ToxID was run automatically after file acquisition using a Xcalibur processing method starting the software tool. The target library was a modified and updated version of the Maurer/Wissenbach/Weber MWW_2014 [23].

LC-HR-MS/MS SUSA

The workup and the LC-HR-MS/MS method were the same as described above for identification of the metabolites. For data evaluation, ThermoFisher TraceFinder Clinical Research 3.2 software was used as described by Helfer et al. [18] with the target library of Maurer et al. (Maurer HH, Meyer MR, Helfer AG, Weber AA (2016) Maurer/Meyer/Helfer/Weber MMHW LC-HR-MS/MS library of drugs, poisons, and their metabolites. Wiley-VCH, Weinheim (Germany), in preparation).

Results and discussion

Phase I and phase II metabolites identified by LC-HR-MS/MS

In analogy to a previous study [9], correlation of the MS/MS spectra of the parent compounds and their metabolites allowed deducing the metabolite structures considering established rules [24]. The spectra are supplied as electronic supplementary material in Fig. S1, S2, and S3, those of the phase II metabolites in Fig. S4, S5, and S6 for 5-F-DALT, 7-Me-DALT, and 5,6-MD-DALT, respectively. The figures contain also the proposed chemical structures, accurate masses of the ions, calculated elemental formulas, and mass error values.

Fragmentation patterns proposed for identification of the phase I metabolites by LC-HR-MS/MS

The basic structure was divided into three sections (Fig. 1) for better description of positions: the aromatic ring (section 1), the ethyl spacer (section 2), and the *N*,*N*-diallylamine (section 3). In the following chapters, important mass spectra fragmentation patterns of 5-F-DALT, 7-Me-DALT, 5,6-MD-DALT, and their phase I metabolites will be discussed in detail. All masses within subsequent paragraphs are the calculated, exact masses.

5-F-DALT

Figure S1, no. 1 shows the spectrum of the parent compound with the protonated molecular ion of *m/z* 259.1605 ($C_{16}H_{20}N_2F^+$) and characteristic fragment ions of *m/z* 162.0714 ($C_{10}H_9NF^+$) and *m/z* 110.0964 ($C_7H_{12}N^+$), representing the ethyl indole residue (section 1+2) and the *N*,*N*-diallylmethanimine residue (section 3) following typical α-cleavage [25].

Specific shifts could be observed for each section. If the structure in section 3 was unmodified fragment ions of *m/z* 110.0964 ($C_7H_{12}N^+$) could be observed (nos. 7-10, and 12-13 in Fig. S1) and if *N*-deallylated (- 40.0313 u) fragment ions of *m/z* 70.0651 ($C_4H_8N^+$) were detected (nos. 3-5). If the structures in sections 1 and 2 were unmodified, fragment ions of *m/z* 162.0714 ($C_{10}H_9NF^+$) were observed (nos. 3 and 11), if mono-hydroxylated (+ 15.9949 u) ions of *m/z* 178.0662 ($C_{10}H_9ONF^+$; nos. 2, 4, 5, 7, and 8), or if dihydroxylated (+ 31.9898 u) ions of *m/z* 194.0612 ($C_{10}H_9O_2NF^+$; nos. 9 and 10) occurred. If the structure in section 1 was modified fragment ions of *m/z* 164.0506 ($C_9H_7ONF^+$; no. 6) or *m/z* 150.0714 ($C_9H_9NF^+$; nos. 2, 4, 5, 7, and 8) could be detected after mono-hydroxylation, fragment ions of *m/z* 166.0299 ($C_8H_5O_2NF^+$; nos. 9 and 10) after dihydroxylation, or fragment ions of *m/z* 182.0248 ($C_8H_5O_3NF^+$; nos. 12-13) after trihydroxylation.

For mono-hydroxylations, the protonated molecules of *m/z* 275.1554 ($C_{16}H_{20}ON_2F^+$) were observed and revealed two isomeric aryl-hydroxy metabolites (nos. 7 and 8). For the three dihydroxylated metabolites, the protonated molecules of *m/z* 291.1503 ($C_{16}H_{20}O_2N_2F^+$) led to two isomeric aryl-dihydroxy metabolites (nos. 9 and 10) and one *N*-oxide with additional hydroxylation in section 3 (no. 11). Identification was proposed by the fragment ions of *m/z* 142.0863 ($C_7H_{12}O_2N^+$: 110.0964 + 31.9899 u) and *m/z* 100.0757 ($C_5H_{10}ON^+$), which represented dihydroxylated *N,N*-diallylmethanimine and mono-hydroxylated *N*-allyl-*N,N*-bis-methylamine, respectively. These fragment ions led to the assumption that both hydroxy groups were in section 3 consistent with observations reported by Michely et al. [9], whereby one oxygen was assumed to represent an *N*-oxide. For confirmation, a typical property of *N*-oxides, namely showing a longer RT compared to its non-oxidized precursor on reversed phase columns, was considered [9]. Unfortunately, the corresponding precursor could not be detected, but the long RT (4.3 min) could be compared to those of all other hydroxy, dihydroxy, and trihydroxy metabolites (RT between 2.0 and 4.1 min) that supported the suggested *N*-oxide detection. Trihydroxylations led to protonated

molecules of *m/z* 307.1452 ($C_{16}H_{20}O_3N_2F^+$) with two detected isomeric spectra. As discussed above, they could be proposed as aryl-trihydroxy metabolites (nos. 12 and 13).

Considering oxidation, a protonated molecule of *m/z* 273.1398 ($C_{16}H_{18}ON_2F^+$) showed a spectrum (no. 6) with different fragmentation pattern compared to other spectra. The fragment ions of *m/z* 232.1006 ($C_{13}H_{13}ON_2F^{+\bullet}$) and *m/z* 191.0615 ($C_{10}H_8ON_2F^+$) represented the loss of both allyl groups followed by loss of hydrocyanic acid, respectively. This fragmentation pattern could be explained by ring closure in accordance to the metabolism of DALT and 5-MeO-DALT [9]. The initial step for this metabolite might have reflected a hydroxylation in the amine α-position, leading to an unstable hemiaminal. This could either degrade, oxidize to an amide, or engage in nucleophilic attack of the indole 2-position with resulting ring closure.

Metabolic *N*-dealkylation (no. 3) led after protonation to a molecule of *m/z* 219.1292 ($C_{13}H_{16}N_2F^+$), further aryl-hydroxylation (nos. 4 and 5) to two protonated molecules of *m/z* 235.1241 ($C_{14}H_{16}ON_2F^+$), and additional subsequent *N*-dealkylation to a *N,N*-bis-deallyl aryl-hydroxy metabolite (no. 2) with a protonated molecule of *m/z* 195.0928 ($C_{10}H_{12}ON_2F^+$).

7-Me-DALT

Figure S2, no. 14 shows the spectrum of the parent compound with the protonated molecular ion of *m/z* 255.1856 ($C_{17}H_{23}N_2^+$) and the characteristic fragment pattern is given by fragment ions of *m/z* 158.0964 ($C_{11}H_{12}N^+$) and *m/z* 143.0730 ($C_{10}H_9N^{+\bullet}$) representing the ethyl or methyl indole residue (sections 1+2), and of *m/z* 110.0964 ($C_7H_{12}N^+$), again representing the *N,N*-diallylmethanimine residue (section 3).

If the structure in section 3 was unmodified, fragment ions could be observed of *m/z* 110.0964 ($C_7H_{12}N^+$; nos. 18, 19, 21-23, 25, 26, and 28 in Fig. S2), if *N*-deallylated ions of *m/z* 70.0651 ($C_4H_8N^+$; nos. 15-17). If the structures in sections 1 and 2 were unmodified, fragment ions of *m/z* 158.0964 ($C_{11}H_{12}N^+$) and *m/z* 143.0730 ($C_{10}H_9N^{+\bullet}$; nos. 15, 20, 24, and 27) appeared, if

mono-hydroxylated shifts to fragment ions of *m/z* 174.0913 ($C_{11}H_{12}ON^+$; nos. 16-20) and/or *m/z* 159.0679 ($C_{10}H_9ON^+$) were observed (nos. 16, 18, and 19), if dihydroxylated, ions of *m/z* 190.0863 ($C_{11}H_{12}O_2N^+$; nos. 22 and 23) and/or *m/z* 162.0550 ($C_9H_8O_2N^+$; no. 23), or if trihydroxylated, ions of *m/z* 206.0812 ($C_{11}H_{12}O_3N^+$; no. 26) appeared. Due to the fact that hydroxylation of the structure in in section 2 led to additional high abundant water losses (- 18.0106 u), the presence or absence of corresponding fragment ions led to the refined position of hydroxylations in section 2 or 1, respectively. After proposed water losses, fragment ions were detected of *m/z* 156.0807 ($C_{11}H_{10}N^+$: 174.0913 - 18.0106 u; no. 17), *m/z* 172.0757 ($C_{11}H_{10}ON^+$: 190.0863 - 18.0106 u; no. 22), or *m/z* 188.0706 ($C_{11}H_{10}O_2N^+$: 206.0812 - 18.0106 u; no. 26). After carboxylation of the methyl group in section 1, fragment ions of *m/z* 188.0706 ($C_{11}H_{10}O_2N^+$; no. 21) occurred. After subsequent mono-hydroxylation (no. 25), corresponding fragment ions could be observed of *m/z* 204.0656 ($C_{11}H_{10}O_3N^+$) or after subsequent dihydroxylation (no. 28) of *m/z* 220.0604 ($C_{11}H_{10}O_4N^+$). It should be mentioned that these fragment ions could also represent ethyl indole structures following water losses as already described, but could be distinguished by considering the precursor molecules and the lack of corresponding fragment ions shifted by +18.0106 u (+ H_2O).

After mono-hydroxylation, three protonated molecules of *m/z* 271.1804 ($C_{17}H_{23}ON_2^+$) could be detected. Two of them were proposed to be aryl-hydroxy metabolites (nos. 18 and 19) and the third isomer might have reflected the *N*-oxide species (no. 20) based on increased retention (4.9 min) compared to the parent compound (4.7 min) as described above. Dihydroxylation led to three isomers with protonated molecules of *m/z* 287.1754 ($C_{17}H_{23}O_2N_2^+$), whereby one isomer was proposed to be an aryl-hydroxy metabolite with additional hydroxylation in section 2 (no. 22), one isomer to be an aryl-dihydroxy metabolite (no. 23), and one to be an *N*-oxide with additional hydroxylation in section 3 (no. 24), identified by the fragment ion of *m/z* 142.0863 ($C_7H_{12}O_2N^+$) as already described above and by longer RT (4.5 min) compared to the other mono- and multi-hydroxy metabolites (RT between 2.9 and 3.9 min). After trihydroxylation, two isomers with protonated molecules of *m/z* 303.1703 ($C_{17}H_{23}O_3N_2^+$) were detected, whereby one isomer was

thought to be an aryl-dihydroxy metabolite with additional hydroxylation in section 2 (no. 26), whereas the other was suggested to be an *N*-oxide with additional dihydroxylation in section 3 (no. 27), identified by fragment ion of *m/z* 158.0957 ($C_{11}H_{12}N^+$), representing unmodified sections 1 and 2. Similarly, the increased RT of 4.7 min was consistent with the proposed *N*-oxidation. Finally, one isomer after fourfold hydroxylation could be detected with the spectrum no. 29 showing a protonated molecule of *m/z* 319.1652 ($C_{17}H_{23}O_4N_2^+$) and a slightly different fragmentation pattern. The fragment ion of *m/z* 144.1019 ($C_7H_{14}O_2N^+$: 110.0964 + 31.9899 + 2.0156 u) represented a dihydroxylated *N,N*-diallylmethanamine (section 3), but with a shift of two hydrogens (+ 2.0156 u) compared to the fragment ion of *m/z* 142.0863 ($C_7H_{12}O_2N^+$) described for spectrum no 24. In addition, the fragment ion of *m/z* 188.0706 ($C_{11}H_{10}O_2N^+$) occurred, representing the ethyl indole structure (section 1+2), but with further double bond in section 2. This led to the assumption that two hydroxy groups were positioned in section 1 and two in section 3, respectively.

Furthermore, the carboxylation following initial hydroxylation at the methyl group in section 1 with further oxidation to a carboxy group (no. 21) could be detected with a protonated molecule of *m/z* 285.1598 ($C_{17}H_{21}O_2N_2^+$). The fragment ion of *m/z* 188.0706 ($C_{11}H_{10}O_2N^+$) represented the ethyl indole structure with the carboxy substituent as described above and the fragment ion of *m/z* 170.0600 ($C_{11}H_8ON^+$) represented the same structure after subsequent loss of water. Similar fragmentation pattern for carboxy substituents at aromatic systems had already been described in previous studies [26] on the NPS 4-methyl-*N*-ethylmethcathinone (4-MEC). Furthermore, subsequent mono-hydroxylation (no. 25) and dihydroxylation (no. 28) in section 1 led to spectra with protonated molecules of *m/z* 301.1547 ($C_{17}H_{21}O_3N_2^+$) or *m/z* 317.1496 ($C_{17}H_{21}O_4N_2^+$) and shifts of +15.9949 u for one oxygen to *m/z* 186.0550 ($C_{11}H_8O_2N^+$) or 202.0499 ($C_{11}H_8O_3N^+$), respectively. An additional fragment ion of *m/z* 192.0291 ($C_9H_6O_4N^+$) could be observed in spectrum no. 28 representing section 1.

N-Dealkylation (no. 15) was detected with a protonated molecule of *m/z* 215.1543 ($C_{14}H_{19}N_2^+$) and after further hydroxylation in two isomeric metabolites with protonated molecules

of *m/z* 231.1492 ($C_{14}H_{19}ON_2^+$). One of these isomers was hydroxylated in section 2 (no. 17). The second isomer showed an additional fragment ion of *m/z* 162.0913 ($C_{10}H_{12}ON^+$), which represented hydroxy methyl indole with hydroxylation taking place in section 1 (no. 16).

5,6-MD-DALT

Figure S3, no. 30 shows the spectrum of the parent compound with the protonated molecule of *m/z* 285.1598 ($C_{17}H_{21}O_2N_2^+$) and the characteristic fragmentation pattern with the fragment ions of *m/z* 188.0706 ($C_{11}H_{10}O_2N^+$) representing the ethyl indole residue (section 1+2), *m/z* 158.0600 ($C_{10}H_8ON^+$) after cleavage of formaldehyde (- 30.0106), and *m/z* 110.0964 ($C_7H_{12}N^+$) for section 3.

Unmodified section 3 led to fragment ions of *m/z* 110.0964 ($C_7H_{12}N^+$; nos. 33-37 in Fig. S3) and if *N*-deallylated (- 40.0313 u) of *m/z* 70.0651 ($C_4H_8N^+$; nos. 31 and 32), unmodified sections 1 and 2 led to fragment ions of *m/z* 188.0706 ($C_{11}H_{10}O_2N^+$) and *m/z* 158.0600 ($C_{10}H_8ON^+$; nos. 31, 36, 38, and 39). If section 1 and 2 were mono-hydroxylated (nos. 32 and 35) fragment ions of *m/z* 204.0656 ($C_{11}H_{10}O_3N^+$: 188.0706 + 15.9949 u), *m/z* 174.0550 ($C_{10}H_8O_2N^+$: 158.0600 + 15.9949 u), *m/z* 176.0342 ($C_9H_6O_3N^+$), and *m/z* 146.0600 ($C_9H_8ON^+$) could be observed.

After mono-hydroxylation, two isomeric metabolites were detected with protonated molecules of *m/z* 301.1547 ($C_{17}H_{21}O_3N_2^+$). One isomer presumably reflected the presence of an aryl-hydroxy metabolite (no. 35) whereas the other isomer was identified as an *N*-oxide (no. 36) with longer RT (4.5 min) than the parent compound (4.3 min). After dihydroxylation, two spectra with protonated molecules of *m/z* 317.1496 ($C_{17}H_{21}O_4N_2^+$) were detected, one proposed aryl-dihydroxy metabolite (no. 37) and one *N*-oxide with further hydroxylation in section 3 (no. 38). Furthermore, one spectrum with a protonated molecule of *m/z* 333.1440 ($C_{17}H_{21}O_5N_2^+$) showed an *N*-oxide with further dihydroxylation in section 3 (no. 39). The spectra showed fragment ions of *m/z* 142.0863 ($C_7H_{12}O_2N^+$: 110.0964 + 31.9899 u) or *m/z* 158.0812 ($C_7H_{12}O_3N^+$: 110.0964 + 47.9848 u), representing di- or trihydroxylated *N*,*N*-diallylmethanimine (section 3). *N*-oxidations

were again proposed due to long RT of 4.0 or 4.2 min compared to those of all hydroxy metabolites (only up to 3.6 min). A further spectrum could be detected after *N*-dealkylation (no. 31) with a protonated molecule of *m/z* 245.1285 ($C_{14}H_{17}O_2N_2^+$), a fragment ion of *m/z* 176.0706 ($C_{10}H_{10}O_2N^+$) representing the ethyl indole residue with two hydroxy groups, which may be formed after cleavage of the methylene group. Furthermore, a fragment ion of *m/z* 146.0600 ($C_9H_8ON^+$) could be observed, what was already described for metabolites with mono-hydroxylated section 1, what seemed to be formed after cleavage of formaldehyde from the methylenedioxy substituent. One *N*-deallyl aryl-hydroxy metabolite (no. 32) was detected with a protonated molecule of *m/z* 261.1234 ($C_{14}H_{17}O_3N_2^+$) and fragment ions, which were already described above.

In addition, a common metabolic step of methylenedioxy compounds was the demethylenation [27]. The resulting metabolite (no. 33) was detected with a protonated molecule of *m/z* 273.1598 ($C_{16}H_{21}O_2N_2^+$). Additional hydroxylation in section 2 with subsequent oxidation led to a spectrum of a demethylenyl oxo metabolite (no. 34) with a protonated molecule of *m/z* 287.1390 ($C_{17}H_{19}O_3N_2^+$) and typical fragmentation pattern in contrast to those after ring closure (no. 6 in Fig.S1).

Fragmentation patterns proposed for identification of the phase II metabolites by LC-HR-MS/MS

Relevant fragmentation patterns of the mass spectra of 5-F-DALT, 7-Me-DALT, and 5,6-MD-DALT phase II metabolites will be presented here with all masses representing the calculated exact masses.

5-F-DALT

After loss of the conjugate moiety (-79.9568 u for sulfates or -176.0321 u for glucuronides) the spectra showed same fragment ions corresponding to those of the underlying phase I metabolites.

Additional fragment ions of *m/z* 258.0231 ($C_{10}H_9O_4NFS^+$; nos. 4S, 5S, and 7S in Fig. S4) were observed for sulfates or ions of *m/z* 354.0984 ($C_{16}H_{17}O_7NF^+$; nos. 4G, 5G, 7G, and 8G) for glucuronides. These fragment ions represented conjugated ethyl indole parts (258.0231: 178.0662 + 79.9568; 354.0984: 178.0662 + 176.0321). In total, sulfates and glucuronides could be detected for one aryl-hydroxy isomer (nos. 7S and 7G) and the two isomers of the *N*-deallyl aryl-hydroxy metabolite (nos. 4S, 5S, 4G, and 5G). For the second aryl-hydroxy isomer (no. 8G), only a glucuronide could be observed.

7-Me-DALT

Glucuronides of the aryl-hydroxy (no. 18G) and the *N*-deallyl alkyl-hydroxy metabolite (no. 17G) were found, but not their sulfates. The *N*-deallyl aryl-hydroxy metabolite formed a glucuronide as well as a sulfate (nos. 16S and 16G in Fig. S5). Again, after loss of the conjugate moiety (-79.9568 u for sulfates or -176.0321 u for glucuronides) the spectra showed same fragment ions corresponding to those of the underlying phase I metabolites plus fragment ions of *m/z* 254.0482 ($C_{11}H_{12}O_4NS^+$; no. 16S) or *m/z* 350.1234 ($C_{17}H_{20}O_7N^+$; nos. 16G, 17G, and 18G) for the ethyl indole moieties (sections 1+2) still carrying sulfate or glucuronide rests.

5,6-MD-DALT

All conjugates resulted from the demethylenyl metabolite, namely one glucuronide (no. 33G), one methyl conjugate (no. 33M in Fig. S6), and one combination of both (no. 33MG). Again, fragment ions of the conjugated ethyl indole moieties (section 1+2) were observed of *m/z* 352.1027 ($C_{16}H_{18}O_8N^+$; no. 33G) or *m/z* 366.1183 ($C_{17}H_{20}O_8N^+$; no. 33MG) in addition to the fragment ions described for the underlying phase I metabolite.

Metabolic pathways proposed according to mass spectral interpretation

The metabolic pathways proposed according to the identified metabolites are depicted in Fig. 2 for 5-F-DALT, in Fig. 3 for 7-Me-DALT, and in Fig. 4 for 5,6-MD-DALT. Numbers correspond to those shown in Fig. S1-6.

5-F-DALT

Aromatic hydroxylations on the indole ring could be expected at four positions but only two of them were detected (7, 8 in Fig. 2). This was most probably caused by either insufficient separation or low abundance of the other isomers. These metabolites were further hydroxylated to two dihydroxy metabolites (9, 10) and these finally to two trihydroxy metabolites (12, 13) at the indole ring, respectively. Furthermore, a ring-rearranged metabolite (6) could be formed after aliphatic hydroxylation in section 2. *N*-Oxidation could only be observed in combination with hydroxylation in section 3 (11). *N*-dealkylation led to metabolite no. 3, which was further hydroxylated in section 1 to two isomeric *N*-deallyl hydroxy metabolites (4, 5) and one of them was subsequently *N*-dealkylated to the *N,N-bis*-deallyl hydroxy metabolite (2).

7-Me-DALT

Aromatic and aliphatic hydroxylations led to two isomeric aryl-hydroxy metabolites (18, 19 in Fig. 3), which were further aliphatically hydroxylated in section 2 (22) or aromatically in section 1 (23). The combination of both led to metabolite no. 26. Further dihydroxylation in section 3 of the metabolite no. 23 finally led to a fourfold hydroxylated metabolite carrying two aromatic and two aliphatic hydroxy groups (29). *N*-Oxidation (20) followed by mono- (24) and dihydroxylation (27) in section 3 could also be observed. Metabolite no. 15 resulted from *N*-dealkylation followed by

aromatic (16) or aliphatic hydroxylation in section 2 (17). Another pathway was the carboxylation after initial hydroxylation of the methyl group in section 1 and subsequent oxidation to the carboxylic acid (21). In addition, this step could be followed by aromatic mono- (25) and dihydroxylation (28).

5,6-MD-DALT

Only aromatic mono- (35 in Fig. 4) and dihydroxylation (37) could be observed in section 1 but no single aliphatic hydroxylation. However, *N*-oxidation (36) with following mono- (38) and dihydroxylation in section 3 (39) could be proposed. In addition, *N*-dealkylation (31) followed by aromatic hydroxylation (32) could be observed as well as *O*-demethylenation (33), typical for demethylenyl structures, which was followed by hydroxylation in section 2 and oxidation to the keto or amide group (34).

Incubations of 5-F-DALT, 7-Me-DALT, and 5,6-MD-DALT with human liver microsomes

To confirm whether the metabolites found in rat urine can also be found in human urine, pHLM incubations were performed providing a good tool for predictions of phase I metabolites that could be detected in human urine as already described in former studies [26, 28-30]. All phase I metabolites could be detected with exception of the *N,N-bis*-deallyl aryl-hydroxy metabolite (no. 2 in Fig. S1) in the case of 5-F-DALT and of the threefold and fourfold hydroxy metabolites (nos. 23, 26, 27, and 29 in Fig. S2) in the case of 7-Me-DALT. the demethylenyl oxo metabolite and the pathway leading to the *N*-dealkylation (nos. 31 and 32 in Fig. S3) could not be confirmed for 5,6-MD-DALT. This fact might be explained by CYP inhibition by 5,6-MD-DALT shown by Dinger et al. [31] who investigated the inhibition potential of methylenedioxy-derived designer drugs and concluded that 5,6-MD-DALT was a strong inhibitor of CYP1A2, CYP2C9, CYP2D6,

and CYP3As. However, it seemed reasonable to assume that at least some of the detected rat metabolites might also be found in human urine for all compounds.

Initial screening for determining the CYP activity

The metabolites were detected after incubation with individual CYPs. The general involvement of the single CYPs in metabolic pathways of 5-F-DALT is given in Table 1, those of 7-Me-DALT in Table 2, and those of 5,6-MD-DALT in Table 3. It should be kept in mind that these qualitative data did not reflect a quantitative contribution of a CYP to the hepatic clearance that would require the collection of enzyme kinetic data [32], which was beyond the scope of this study. According to these findings, the following isoenzymes were generally involved in the given metabolic steps: for 5-F-DALT, CYP1A2, CYP2B6, CYP2D6, and CYP3A4 in all types of hydroxylations, CYP1A2 and CYP2D6 in oxidation to the oxo metabolite, CYP 1A2, CYP2C9, CYP2C19, CYP2D6, and CYP3A4 in *N*-dealkylations; for 7-Me-DALT, CYP2B6 and CYP3A4 in all types of hydroxylations, CYP2D6 and CYP3A5 in oxidation to the carboxy metabolites, and CYP1A2, CYP2B6, CYP2C9, CYP2C19, and CYP3A4 in *N*-dealkylations; for 5,6-MD-DALT, CYP3A4 in all types of hydroxylations, CYP1A2, CYP2C9, and CYP3A4 in demethylenations, and CYP1A2, CYP2C9, CYP2D6, and CYP3A4 in *N*-dealkylations. The inhibition potential of 5,6-MD-DALT on these CYPs [31] could be responsible for not detecting the corresponding metabolites in pHLM incubations.

GC-MS, LC-MS^n, and LC-HR-MS/MS screening for detection of 5-F-DALT, 7-Me-DALT, and 5,6-MD-DALT

Due to the fact that the investigated compounds did not yet appear on the market, no human doses are known. Nevertheless, the known and misused derivative 5-MeO-DALT might be taken into

consideration with suggested human doses of about 10 mg [33-35]. After scaling by dose-by-factor approach according to Sharma et al. [36], such doses would correspond to 1 mg/kg BM administered to rats. The corresponding urine samples were used for the detectability studies. As the drug potency might be higher, the expected users' dose could also be lower than 10 mg. Hence, rat urine analysis following drug administration of 0.1 mg/kg BM was included in order to verify reliable detection. All targets found in rat urine after 1 or 0.1 mg/kg BM administration using GC-MS are given in Table 4 with the corresponding fragment ions, their relative abundances, and their retention indices. The targets using LC-MS^n are shown in Table 5 with the protonated precursor ions, characteristic MS^2 and MS^3 fragment ions, and retention times. The reference spectra for GC-MS and LC-MS^n monitoring are published elsewhere [21, 23]. In Table 6, the targets using LC-HR-MS/MS are shown in an overview of compounds found in all three SUSAs in the two different doses and the corresponding spectra are depicted in supplementary data Figs. S1-6.

In the GC-MS screening, 5-F-DALT and 7-Me-DALT could be detected, but not 5,6-MD-DALT when administering the 1 mg/kg BM dose. The 0.1 mg/kg BM dose did not allow for the detection of the test drugs although they could be monitored after high dose administration and might therefore be detectable in overdose cases. The LC-MS^n screening allowed detection of all drugs after 1 mg/kg BM administrations and only 5-F-DALT enabled monitoring at the 0.1 mg/kg BM dose. The LC-HR-MS/MS procedure revealed the ability to monitor all drugs after the 1 mg/kg BM doses although only 5-F-DALT and 7-Me-DALT following the 0.1 mg/kg BM doses. Thus, 5,6-MD-DALT could not be monitored after the 0.1 mg/kg BM dose by the three SUSAs, which highlighted a challenge, for example, in cases where this drug would be consumed in such small doses.

The most abundant metabolites following work-up of a rat urine sample after the 1 mg/kg BM dose are depicted in Fig. 5 as reconstructed LC-HR-MS ion chromatograms with the given *m/z* values. The most abundant peaks of 5-F-DALT (part A) were the aryl-hydroxy metabolite (7) and

the two isomers of the aryl-hydroxy glucuronide (7G and 8G), those of 7-Me-DALT (part B) the *N*-deallyl aryl-hydroxy (16), the carboxy (21), and the aryl-dihydroxy metabolite (23), and those of 5,6-MD-DALT (part C) the demethylenyl (33), the demethylenyl oxo (34), and the demethylenyl glucuronide metabolite (33G). These results showed that a reliance on the parent molecule alone, at least when working with urine samples [15] following the investigated doses, might carry the risk of providing false negative results without including the targeted analysis of their biotransformation products.

Conclusions

The three substances 5-F-DALT, 7-Me-DALT, and 5,6-MD-DALT might be considered as possible replacements of already misused tryptamine-based NPS in the event of their scheduling. They showed an extensive biotransformation in rats. Results obtained from pHLM incubations suggested that that most metabolites might also be detectable in human urine. CYP1A2, CYP 2B6, CYP2C9, CYP2C19, CYP2D6, CYP3A4, and CYP3A5 were generally involved in the main pathways. GC-MS did not allow a reliable monitoring of suspected consumption although it is suspected that this should be overcome in the event of larger doses or overdose cases. The LC-MS^n and LC-HR-MS/MS SUSAs were suitable for monitoring consumption of all three compounds, but only via their metabolites. Very low doses administered to male Wistar rats (0.1 mg/kg BM) revealed the ability of LC-HR-MS/MS to monitor 5-F-DALT and 7-Me-DALT, whereas 5-F-DALT could be monitored using LC-MS^n. However, when a 1 mg/kg BM dose was administered, all drugs could be monitored by LC-HR-MS/MS and LC-MS^n.

Acknowledgements The authors like to thank Achim T. Caspar, Julia Dinger, Andreas G. Helfer, Jessica Welter, Carina S. D. Wink, Carsten Schröder, Gabriele Ulrich, and Armin A. Weber for their support and/or helpful discussion.

Conflict of interest

The authors declare that there are no conflicts of interest.

Compliance with Ethical Standards

The authors declare that the experiments have been conducted in accordance with animal ethical care.

References

1. Brandt SD, King LA, Evans-Brown M (2014) The new drug phenomenon. Drug Test Anal 6:587-597
2. United Nations Office on Drugs and Crime (UNODC) (2014) World Drug Report 2014. http://www.unodc.org/documents/data-and-analysis/WDR2014/World_Drug_Report_2014_web.pdf
3. United Nations Office on Drugs and Crime (UNODC) (2015) World Drug Report 2015. https://www.unodc.org/documents/wdr2015/World_Drug_Report_2015.pdf
4. United Nations Office on Drugs and Crime (UNODC) (2016) World Drug Report 2016. https://www.unodc.org/doc/wdr2016/WORLD_DRUG_REPORT_2016_web.pdf
5. Palamar JJ, Martins SS, Su MK, Ompad DC (2015) Self-reported use of novel psychoactive substances in a US nationally representative survey: Prevalence, correlates, and a call for new survey methods to prevent underreporting. Drug Alcohol Depend 156:112-119
6. Sanders B, Lankenau SE, Bloom JJ, Hathazi D (2008) "Research chemicals": tryptamine and phenethylamine use among high-risk youth. Subst Use Misuse 43:389-402
7. Corkery JM, Durkin E, Elliott S, Schifano F, Ghodse AH (2012) The recreational tryptamine 5-MeO-DALT (N,N-diallyl-5-methoxytryptamine): a brief review. Prog Neuropsychopharmacol Biol Psychiatry 39:259-262
8. Jovel A, Felthous A, Bhattacharyya A (2014) Delirium due to intoxication from the novel synthetic tryptamine 5-MeO-DALT. J Forensic Sci 59:844-846
9. Michely JA, Helfer AG, Brandt SD, Meyer MR, Maurer HH (2015) Metabolism of the new psychoactive substances N,N-diallyltryptamine (DALT) and 5-methoxy-DALT and their detectability in urine by GC-MS, LC-MSn, and LC-HR-MS/MS. Anal Bioanal Chem 407:7831-7842

10. Meyer MR, Maurer HH (2016) Review: LC coupled to low- and high-resolution mass spectrometry for new psychoactive substance screening in biological matrices - Where do we stand today? Anal Chim Acta 927:12-20
11. Peters FT (2014) Recent developments in urinalysis of metabolites of new psychoactive substances using LC-MS. Bioanalysis 6:2083-2107
12. Brandt SD, Tirunarayanapuram SS, Freeman S, Dempster N, Barker SA, Daley PF, Cozzi NV, Martins CPB (2008) Microwave-accelerated synthesis of psychoactive deuterated N,N-dialkylated-[alpha,alpha,beta,beta-d(4)]-tryptamines. J Label Compd Radiopharm 51:423-429
13. Cozzi NV, Daley PF (2016) Receptor binding profiles and quantitative structure-affinity relationships of some 5-substituted-N,N-diallyltryptamines. Bioorg Med Chem Lett 26:959-964
14. Brandt SD, Kavanagh PV, Dowling G, Talbot B, Westphal F, Meyer MR, Maurer HH, Halberstadt AL (2016) Analytical characterization of N,N-diallyltryptamine (DALT) and 16 ring-substituted derivatives. Drug Test Anal DOI: 10.1002/dta.1974
15. Meyer MR, Caspar A, Brandt SD, Maurer HH (2014) A qualitative/quantitative approach for the detection of 37 tryptamine-derived designer drugs, 5 beta-carbolines, ibogaine, and yohimbine in human urine and plasma using standard urine screening and multi-analyte approaches. Anal Bioanal Chem 406:225-237
16. Maurer HH, Pfleger K, Weber AA (2016) Mass spectral data of drugs, poisons, pesticides, pollutants and their metabolites. Wiley-VCH, Weinheim (Germany)
17. Wissenbach DK, Meyer MR, Remane D, Philipp AA, Weber AA, Maurer HH (2011) Drugs of abuse screening in urine as part of a metabolite-based LC-MS(n) screening concept. Anal Bioanal Chem 400:3481-3489
18. Helfer AG, Michely JA, Weber AA, Meyer MR, Maurer HH (2015) Orbitrap technology for comprehensive metabolite-based liquid chromatographic-high resolution-tandem mass

spectrometric urine drug screening - exemplified for cardiovascular drugs. Anal Chim Acta 891:221-233

19. Wissenbach DK, Meyer MR, Remane D, Weber AA, Maurer HH (2011) Development of the first metabolite-based LC-MSn urine drug screening procedure - exemplified for antidepressants. Anal Bioanal Chem 400:79-88
20. Meyer MR, Vollmar C, Schwaninger AE, Maurer HH (2012) New cathinone-derived designer drugs 3-bromomethcathinone and 3-fluoromethcathinone: studies on their metabolism in rat urine and human liver microsomes using GC-MS and LC-high-resolution MS and their detectability in urine. J Mass Spectrom 47:253-262
21. Maurer HH, Pfleger K, Weber AA (2016) Mass spectral library of drugs, poisons, pesticides, pollutants and their metabolites. Wiley-VCH, Weinheim (Germany)
22. Meyer MR, Peters FT, Maurer HH (2010) Automated mass spectral deconvolution and identification system for GC-MS screening for drugs, poisons, and metabolites in urine. Clin Chem 56:575-584
23. Maurer HH, Wissenbach DK, Weber AA (2014) Maurer/Wissenbach/Weber MWW LC-MSn Library of Drugs, Poisons, and their Metabolites. Wiley-VCH, Weinheim (Germany)
24. Niessen WMA (2011) Fragmentation of Toxicologically Relevant Drugs in Positive-Ion Liquid Chromatography-Tandem Mass Spectrometry. Mass Spectrometry Reviews 30:626-663
25. Brandt SD, Martins CPB (2010) Analytical methods for psychoactive *N*,*N*-dialkylated tryptamines. Trends Anal Chem 29:858-869
26. Helfer AG, Turcant A, Boels D, Ferec S, Lelievre B, Welter J, Meyer MR, Maurer HH (2015) Elucidation of the metabolites of the novel psychoactive substance 4-methyl-*N*-ethyl-cathinone (4-MEC) in human urine and pooled liver microsomes by

GC-MS and LC-HR-MS/MS techniques and of its detectability by GC-MS or LC-MS^n standard screening approaches. Drug Test Anal 7:368-375

27. Meyer MR, Maurer HH (2010) Metabolism of designer drugs of abuse: An updated review [review]. Curr Drug Metab 11:468-482
28. Caspar AT, Helfer AG, Michely JA, Auwaerter V, Brandt SD, Meyer MR, Maurer HH (2015) Studies on the metabolism and toxicological detection of the new psychoactive designer drug 2-(4-iodo-2,5-dimethoxyphenyl)-N-[(2-methoxyphenyl)methyl]ethanamine (25I-NBOMe) in human and rat urine using GC-MS, LC-MSn, and LC-HR-MS/MS. Anal Bioanal Chem 407:6697-6719
29. Wink CSD, Meyer MR, Braun T, Turcant A, Maurer HH (2015) Biotransformation and detectability of the designer drug 2,5-dimethoxy-4-propylphenethylamine (2C-P) studied in urine by GC-MS, LC-MS^n and LC-high resolution-MS^n. Anal Bioanal Chem 407:831-843
30. Wohlfarth A, Roman M, Andersson M, Kugelberg FC, Diao X, Carlier J, Eriksson C, Wu X, Konradsson P, Josefsson M, Huestis MA, Kronstrand R (2016) 25C-NBOMe and 25I-NBOMe metabolite studies in human hepatocytes, in vivo mouse and human urine with high-resolution mass spectrometry. Drug Test Anal DOI: 10.1002/dta.2044
31. Dinger J, Meyer MR, Maurer HH (2016) In vitro cytochrome P450 inhibition potential of methylenedioxy-derived designer drugs studied with a two cocktail approach. Arch Toxicol 90:305-318
32. Wink CSD, Meyer GMJ, Meyer MR, Maurer HH (2015) Toxicokinetics of lefetamine and derived diphenylethylamine designer drugs - Contribution of human cytochrome P450 isozymes to their main phase I metabolic steps. Toxicol Lett 238:39-44
33. Shulgin AT (2003) Basic Pharmacology and Effects. In: Laing, R. R. Halluinogens. A Forensic Drug Handbook. Elsevier Science, London 67-137

34. Shulgin AT, Shulgin A (2004) 5-MeO-DALT. http://isomerdesign.com/PiHKAL/read.php?domain=tk&id=56

35. Shulgin AT, Shulgin A (2004) DALT. http://isomerdesign.com/PiHKAL/read.php?domain=tk&id=57

36. Sharma V, McNeill JH (2009) To scale or not to scale: the principles of dose extrapolation. Br J Pharmacol 157:907-921

37. Kovats E (1958) Gaschromatographische Charakterisierung organischer Verbindungen. Teil 1. Retentionsindices aliphatischer Halogenide, Alkohole, Aldehyde und Ketone. Helv Chim Acta 41:1915-1932

Table 1 General involvement of human CYP isoenzymes in metabolic pathways of 5-F-DALT

CYP isoenzyme	**Hydroxylation, all types**	**Oxidation to oxo metabolites**	***N*-dealkylation**
CYP1A2	+	+	+
CYP2A6			
CYP2B6	+		
CYP2C8			
CYP2C9			+
CYP2C19			+
CYP2D6	+	+	+
CYP2E1			
CYP3A4	+		+
CYP3A5			

Table 2 General involvement of human CYP isoenzymes in metabolic pathways of 7-Me-DALT

CYP isoenzyme	**Hydroxylation, all types**	**Oxidation to carboxy metabolites**	***N*-dealkylation**
CYP1A2			+
CYP2A6			
CYP2B6	+		+
CYP2C8			
CYP2C9			+
CYP2C19			+
CYP2D6		+	
CYP2E1			
CYP3A4	+		+
CYP3A5		+	

Table 3 General involvement of human CYP isoenzymes in metabolic pathways of 5,6-MD-DALT

CYP isoenzyme	**Hydroxylation, all types**	**Demethylenation**	***N*-dealkylation**
CYP1A2		+	+
CYP2A6			
CYP2B6			
CYP2C8			
CYP2C9		+	+
CYP2C19			
CYP2D6			+
CYP2E1			
CYP3A4	+	+	+
CYP3A5			

Table 4 Targets for GC-MS SUSA monitoring 5-F-DALT and 7-Me-DALT with molecular masses, five most abundant fragment ions, their relative abundances, and retention indices according to Kovats [37], numbering according to Fig. 2-4

No.	Target for SUSA	Molecular mass, u	GC-MS fragment ions, *m/z,* and their relative intensities, %	Retention index
7/8	5-F-DALT-M (HO-aryl-) AC	316	110 (100), 164 (7), 68 (4), 81 (3), 178 (3)	2300
18/19	7-Me-DALT-M (HO-aryl-) AC	312	110 (100), 160 (10), 159 (4), 130 (4), 283 (3)	2450
3	7-Me-DALT-M (*N*-dealkyl-HO-aryl-) 2AC	314	173 (100), 215 (62), 160 (55), 70 (30), 202 (25)	2630

Table 5 Targets for LC-MS^n SUSA monitoring 5-F-DALT, 7-Me-DALT, and 5,6-MD-DALT with protonated precursor ions, characteristic MS^2 and MS^3 fragment ions, and retention times (RT), numbering according to Fig. 2-4

No.	Target for SUSA	Precursor ion, *m/z*	MS^2 fragment ions, *m/z,* and relative intensities, %	MS^3 fragment ions, *m/z,* and relative intensities, %	RT, min
4	5-F-DALT-M (*N*-dealkyl-HO-aryl-) isomer 1	235	178 (100), 166 (82), 70 (3)	178: 130 (100), 150 (76), 103 (36), 178 (30), 134 (14)	5.2
5	5-F-DALT-M (*N*-dealkyl-HO-aryl-) isomer 2	235	178 (100), 166 (6)	178: 150 (100), 130 (20), 178 (11), 151 (11), 133 (10)	6.8
6	5-F-DALT-M (oxo-)	273	232 (100)	232: 191 (100)	10.1
7	5-F-DALT-M (HO-aryl-) isomer 1	275	110 (100), 178 (5), 233 (1)	110: 81 (100), 68 (53), 79 (25), 71 (13), 56 (11)	7.2
8	5-F-DALT-M (HO-aryl-) isomer 2	275	178 (100), 110 (76), 98 (10), 239 (2), 233 (2)	178: 178 (100), 123 (92), 150 (67), 130 (45), 140 (33)	9.2
4G	5-F-DALT-M (*N*-dealkyl-HO-aryl-glucuronide) isomer 1	411	354 (100), 166 (76), 178 (36), 235 (13), 342 (12)	354: 178 (100), 158 (2), 130 (2), 150 (1)	3.0
5G	5-F-DALT-M (*N*-dealkyl-HO-aryl-glucuronide) isomer 2	411	354 (100), 178 (52), 235 (41), 342 (11), 150 (5)	354: 178 (100)	5.0
7G	5-F-DALT-M (HO-aryl-glucuronide) isomer 1	451	354 (100), 275 (81), 321 (66), 391 (35), 178 (27)	-	4.5
8G	5-F-DALT-M (HO-aryl-glucuronide) isomer 2	451	354 (100), 178 (52), 275 (47), 416 (13), 394 (7)	-	4.8
16	7-Me-DALT-M (*N*-dealkyl-HO-aryl-)	231	350 (100), 162 (91), 338 (53), 174 (47), 231 (33)	350: 174 (100), 159 (3), 146 (1)	5.2
21	7-Me-DALT-M (carboxy-)	285	188 (100), 110 (93), 170 (17), 207 (8), 189 (5)	188: 142 (100), 160 (25), 143 (14), 162 (13), 170 (9)	9.5
23	7-Me-DALT-M (di-HO-aryl-)	287	190 (100), 245 (57), 110 (30), 162 (27), 251 (19)	190: 162 (100), 163 (9), 145 (8), 190 (3), 148 (2)	7.2
26	7-Me-DALT-M (HO-alkyl-di-HO-aryl-)	303	110 (100), 261 (4), 206 (3), 257 (3), 267 (2)	110: 81 (100), 80 (79), 67 (62), 77 (58), 68	4.9

No.	Target for SUSA	Precursor ion, *m/z*	MS^2 fragment ions, *m/z,* and relative intensities, %	MS^3 fragment ions, *m/z,* and relative intensities, %	RT, min
				(28)	
29	7-Me-DALT-M (di-HO-alkyl-di-HO-aryl-)	319	144 (100), 188 (82), 132 (27), 170 (23), 155 (2)	144: 84 (100), 71 (1)	6.9
16G	7-Me-DALT-M (*N*-dealkyl-HO-aryl-glucuronide)	407	350 (100), 162 (91), 338 (53), 174 (47), 231 (33)	350: 174 (100), 159 (3), 146 (1)	3.5
17G	7-Me-DALT-M (*N*-dealkyl-HO-alkyl-glucuronide)	407	350 (100), 231 (83), 174 (61), 156 (49), 144 (20)	350: 156 (100), 174 (45), 154 (2), 129 (1)	5.8
18G	7-Me-DALT-M (HO-aryl-glucuronide)	447	350 (100), 271 (32), 148 (5), 324 (3), 174 (3)	350: 174 (100), 175 (2)	5.0
38	5,6-MD-DALT-M (*N*-oxide-HO-alkyl-)	317	142 (100), 188 (16), 100 (3)	142: 100 (100), 84 (58), 83 (7), 71 (3), 74 (2)	8.1
33G	5,6-MD-DALT-M (demethylenyl-glucuronide)	449	352 (100), 273 (4), 176 (3), 130 (1)	352: 176 (100), 158 (7), 130 (1), 237 (1)	4.4
33MG	5,6-MD-DALT-M (demethylenyl-methyl-glucuronide)	463	287 (100), 366 (16), 190 (13), 158 (3), 418 (2)	287: 110 (100), 190 (13), 193 (1)	4.7

Table 6 Compounds for SUSA using GC-MS, LC-MS^n, and LC-HR-MS/MS monitoring 5-F-DALT, 7-Me-DALT, and 5,6-MD-DALT after doses of 1 or 0.1 mg/kg BM administered to rat, brackets indicate unclear isomer, numbering according to Fig. 2-4

No.	Compound for SUSA	GC-MS		LC-MS^n		LC-HR-MS/MS	
		0.1	**1**	**0.1**	**1**	**0.1**	**1**
4	5-F-DALT-M (*N*-dealkyl-HO-aryl-) isomer 1			+	+	+	+
5	5-F-DALT-M (*N*-dealkyl-HO-aryl-) isomer 2				+		+
6	5-F-DALT-M (oxo-)			+	+	+	+
7	5-F-DALT-M (HO-aryl-) isomer 1		+	+	+	+	+
8	5-F-DALT-M (HO-aryl-) isomer 2				+		+
11	5-F-DALT-M (*N*-oxide-HO-alkyl-)						+
4S	5-F-DALT-M (*N*-dealkyl-HO-aryl-sulfate) isomer 1						+
5S	5-F-DALT-M (*N*-dealkyl-HO-aryl-sulfate) isomer 2						+
7S	5-F-DALT-M (HO-aryl-sulfate)						+
4G	5-F-DALT-M (*N*-dealkyl-HO-aryl-glucuronide) isomer 1				+		+
5G	5-F-DALT-M (*N*-dealkyl-HO-aryl-glucuronide) isomer 2				+		+
7G	5-F-DALT-M (HO-aryl-glucuronide) isomer 1				+		+
8G	5-F-DALT-M (HO-aryl-glucuronide) isomer 2				+		+
16	7-Me-DALT-M (*N*-dealkyl-HO-aryl-)		+		+	+	+
17	7-Me-DALT-M (*N*-dealkyl-HO-alkyl-)						+
18	7-Me-DALT-M (HO-aryl-) isomer 1		+				+

No.	Compound for SUSA	GC-MS		LC-MS^n		LC-HR-MS/MS	
		0.1	1	0.1	1	0.1	1
19	7-Me-DALT-M (HO-aryl-) isomer 2						+
21	7-Me-DALT-M (carboxy-)				+		+
23	7-Me-DALT-M (di-HO-aryl-)				+		+
24	7-Me-DALT-M (*N*-oxide-HO-alkyl-)						+
25	7-Me-DALT-M (HO-aryl-carboxy)						+
26	7-Me-DALT-M (HO-alkyl-di-HO-aryl-)				+		+
28	7-Me-DALT-M (di-HO-aryl-carboxy)						+
29	7-Me-DALT-M (di-HO-alkyl-di-HO-aryl-)				+		+
16S	7-Me-DALT-M (*N*-dealkyl-HO-aryl-sulfate)						+
16G	7-Me-DALT-M (*N*-dealkyl-HO-aryl-glucuronide)				+	+	+
17G	7-Me-DALT-M (*N*-dealkyl-HO-alkyl-glucuronide)				+		+
18G	7-Me-DALT-M (HO-aryl-glucuronide)				+		+
33	5,6-MD-DALT-M (demethylenyl-)						+
34	5,6-MD-DALT-M (demethylenyl-oxo-)						+
38	5,6-MD-DALT-M (*N*-oxide-HO-alkyl-)				+		+
33G	5,6-MD-DALT-M (demethylenyl-glucuronide)				+		+
33MG	5,6-MD-DALT-M (demethylenyl-methyl-glucuronide)				+		+

Legends to Figures

Fig. 1 Structure of 5-F-DALT (part A), 7-Me-DALT (part B), and 5,6-MD-DALT (part C) with corresponding division into sections to aid the identification procedure of metabolites

Fig. 2 Proposed metabolic pathways for 5-F-DALT (numbering according to Fig. S1)

Fig. 3 Proposed metabolic pathways for 7-Me-DALT (numbering according to Fig. S2)

Fig. 4 Proposed metabolic pathways for 5,6-MD-DALT (numbering according to Fig. S3)

Fig. 5 Reconstructed LC-HR-MS ion chromatograms with the corresponding protonated molecular exact masses (± 5 ppm) indicating 5-F-DALT (part A), 7-Me-DALT (part B), or 5,6-MD-DALT metabolites (part C) in rat urine samples after 1 mg/kg BM low dose administration (numbering according to Fig. S1-3)

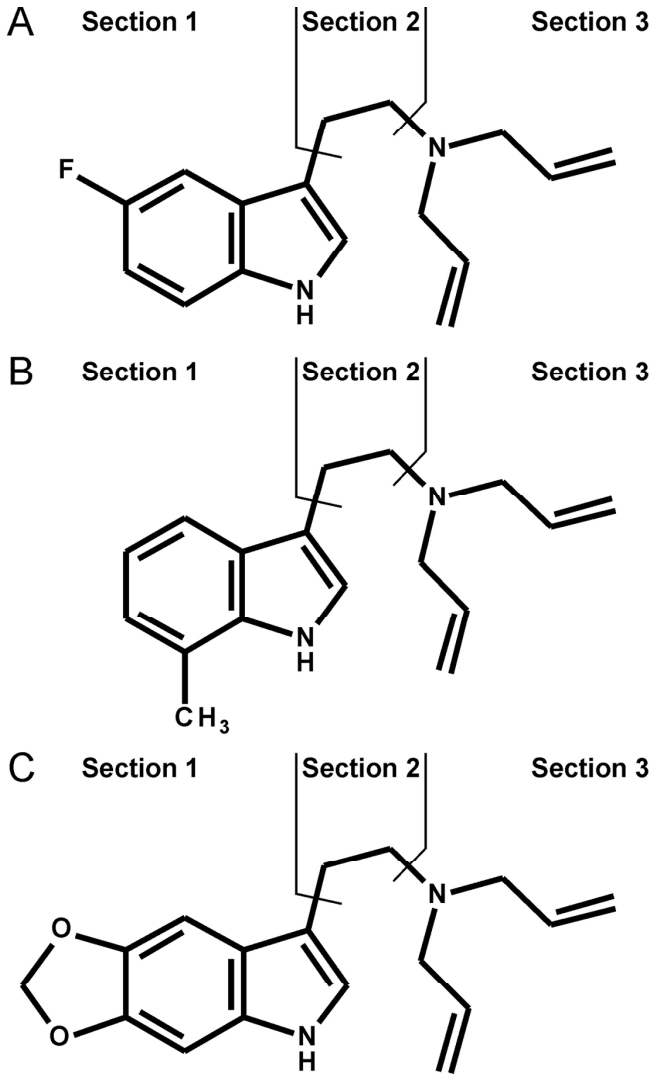

Fig. 1 Structure of 5-F-DALT (part A), 7-Me-DALT (part B), and 5,6-MD-DALT (part C) with corresponding division into sections to aid the identification procedure of metabolites

116x193mm (300 x 300 DPI)

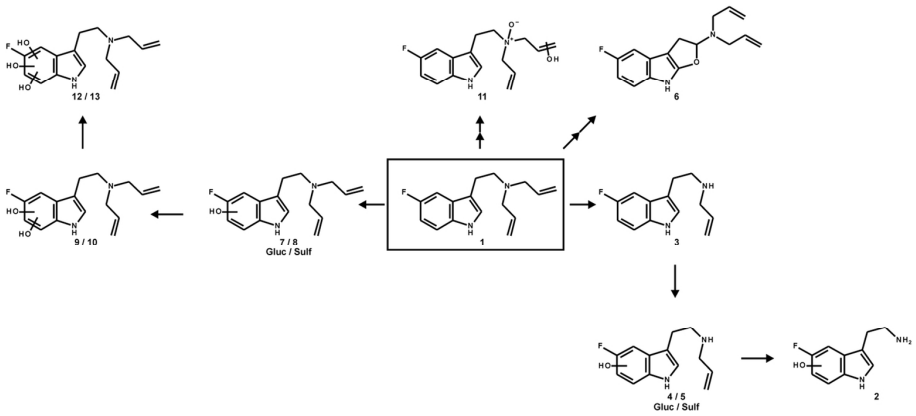

Fig. 2 Proposed metabolic pathways for 5-F-DALT (numbering according to Fig. S1)

126x57mm (300 x 300 DPI)

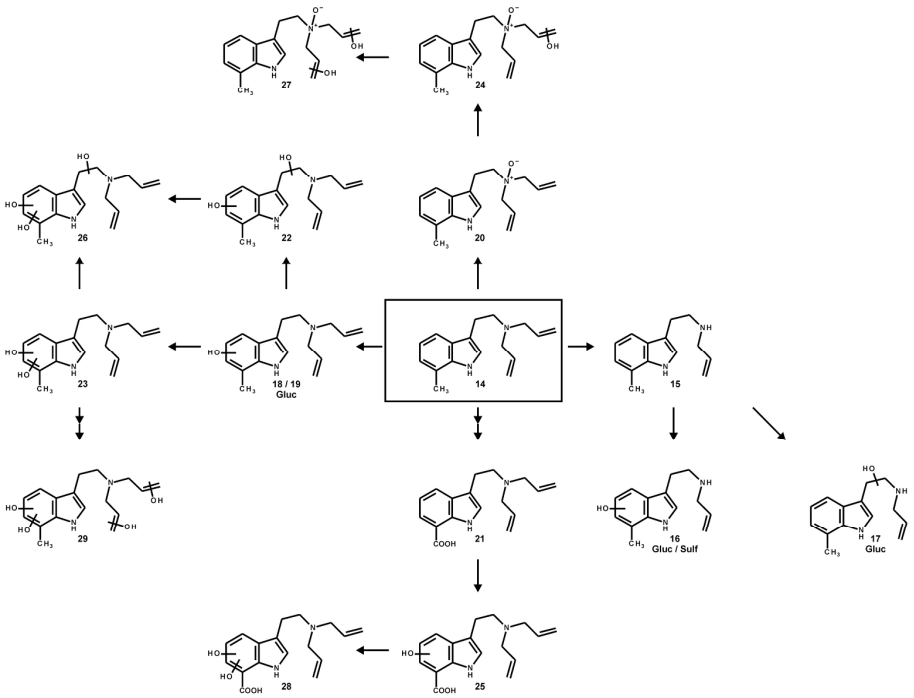

Fig. 3 Proposed metabolic pathways for 7-Me-DALT (numbering according to Fig. S2)

214x163mm (300 x 300 DPI)

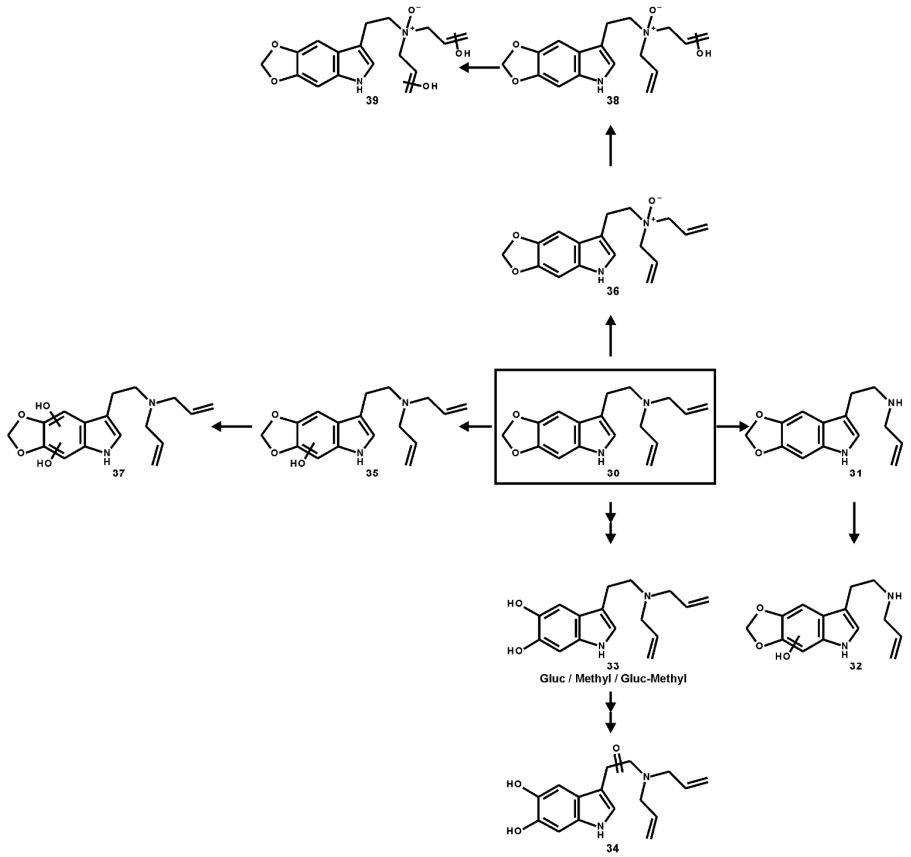

Fig. 4 Proposed metabolic pathways for 5,6-MD-DALT (numbering according to Fig. S3)

224x209mm (300 x 300 DPI)

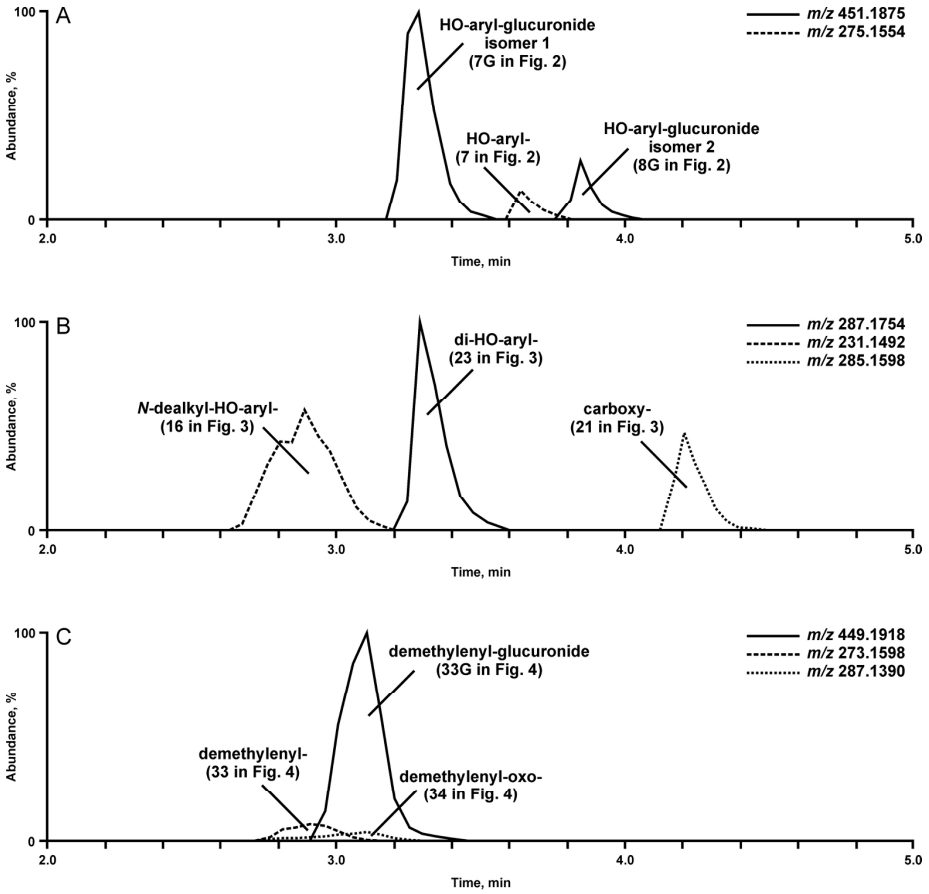

Fig. 5 Reconstructed LC-HR-MS ion chromatograms with the corresponding protonated molecular exact masses (± 5 ppm) indicating 5-F-DALT (part A), 7-Me-DALT (part B), or 5,6-MD-DALT metabolites (part C) in rat urine samples after 1 mg/kg BM low dose administration (numbering according to Fig. S1-3)

192x186mm (300 x 300 DPI)

Analytical and Bioanalytical Chemistry

Electronic Supplementary Material

Metabolism and detectability of the new psychoactive substances *N,N*-diallyltryptamine (DALT) derivatives 5-fluoro-DALT, 7-methyl-DALT, and 5,6-methylenedioxy-DALT in urine using GC-MS, LC-MS^n, and LC-HR-MS/MS

Julian A. Michely * Simon D. Brandt * Markus R. Meyer * Hans H. Maurer

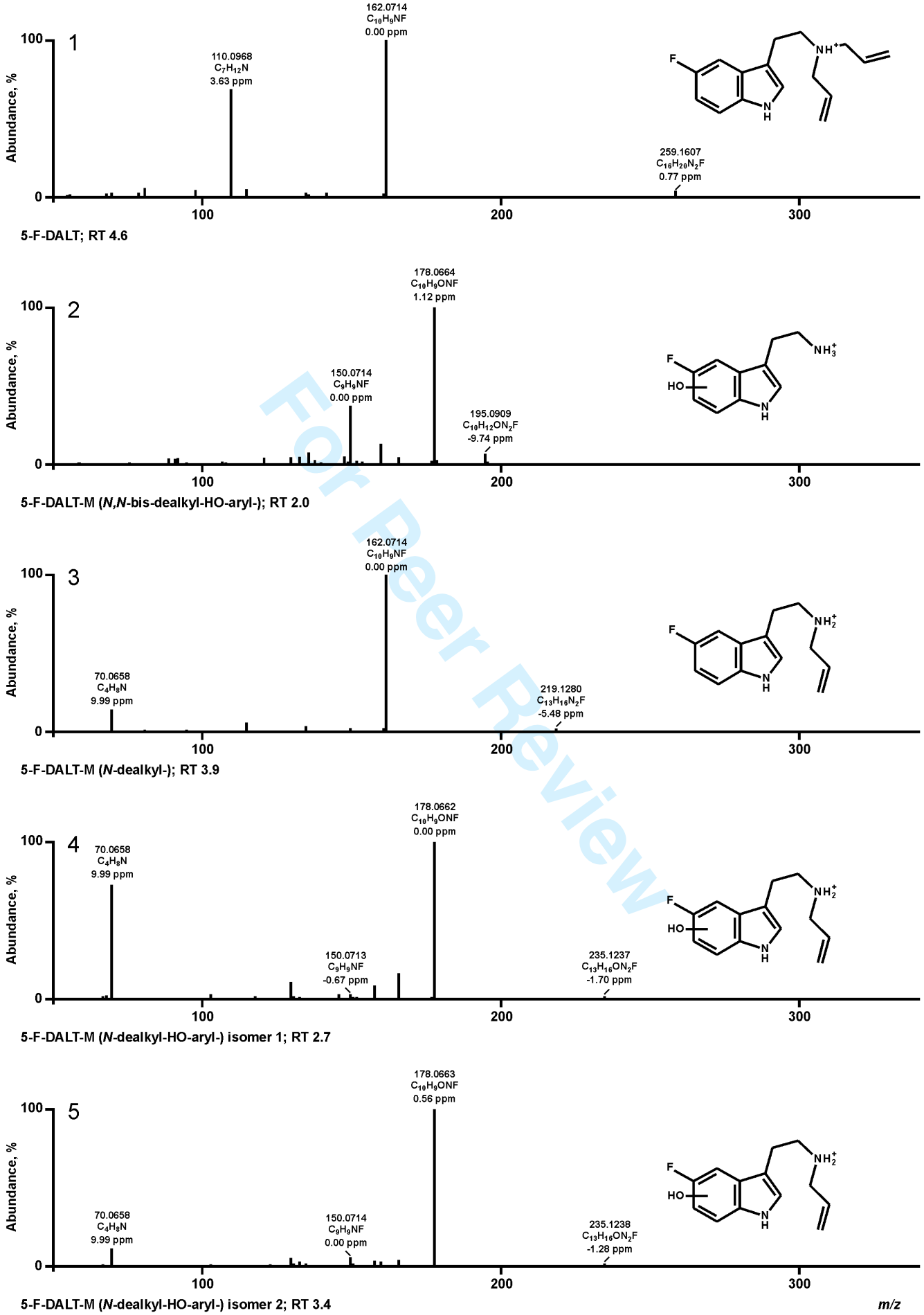

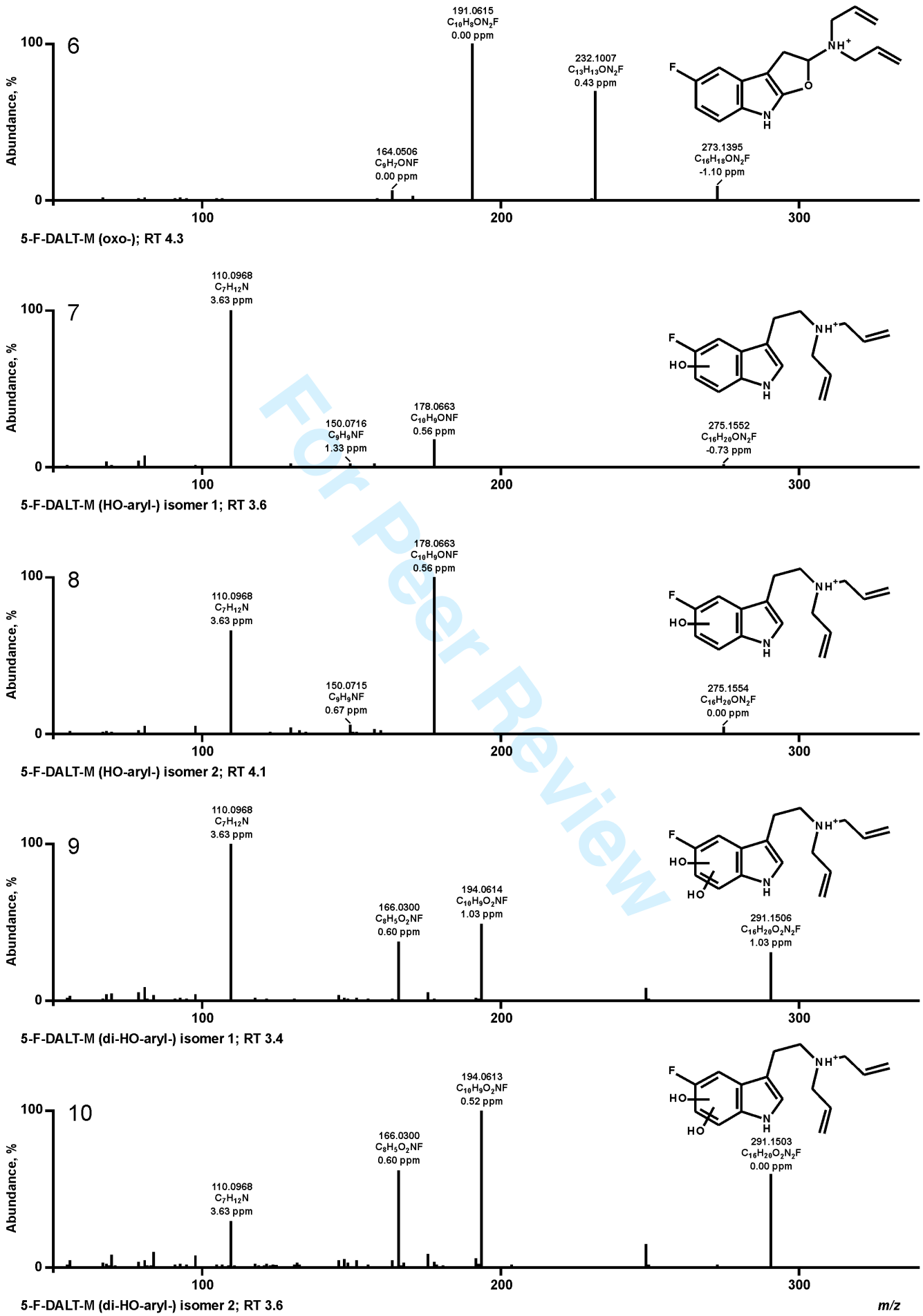

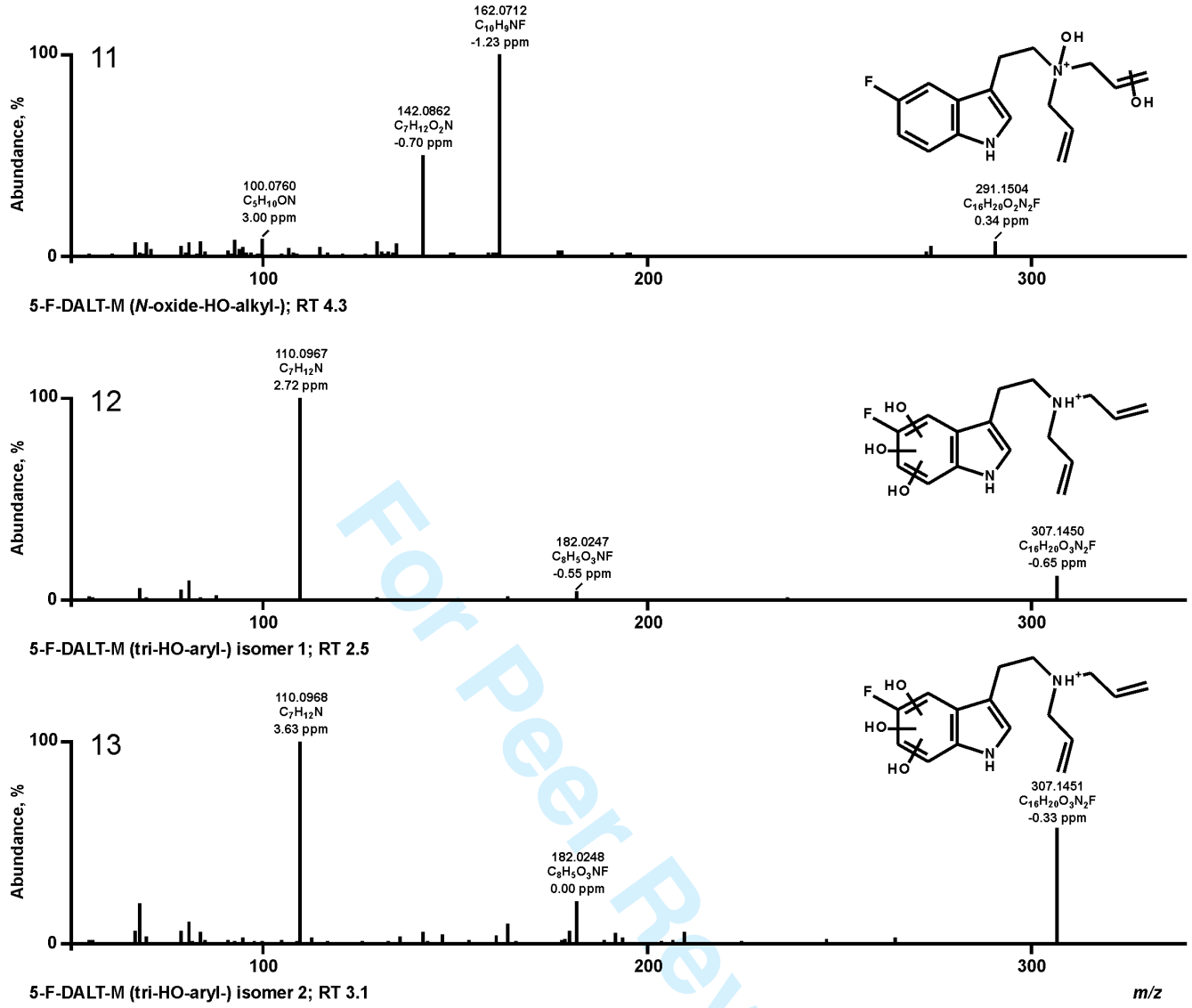

Fig. S1 LC-HR-MS/MS spectra of 5-F-DALT and its phase I metabolites arranged according to their precursor values, proposed chemical structures, accurate masses, calculated elemental formulas, mass error values in parts per million (ppm), and retention times in minutes (min)

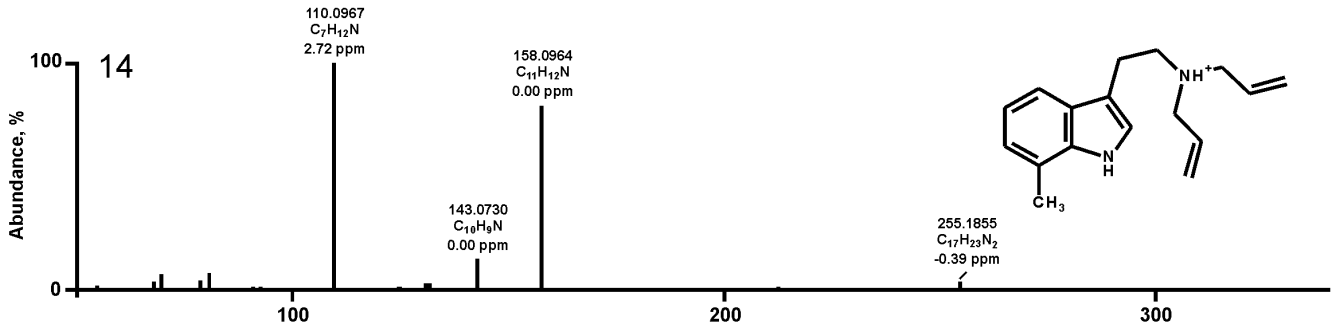

7-Me-DALT; RT 4.7

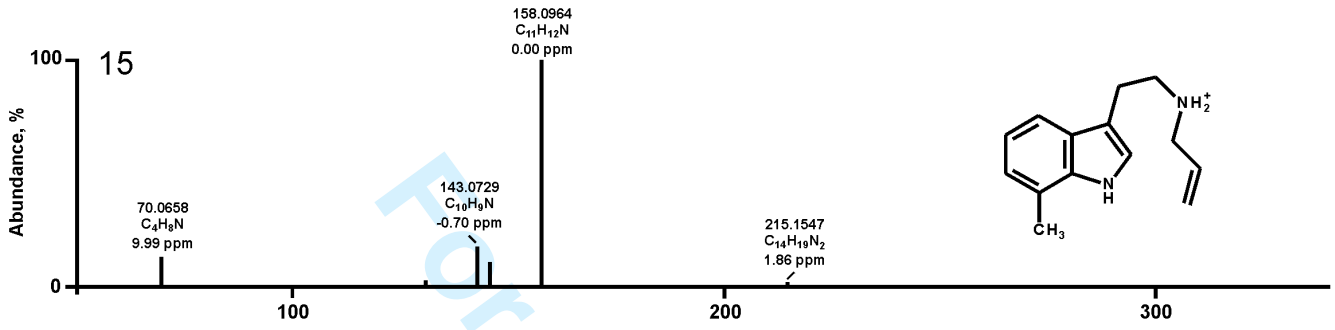

7-Me-DALT-M (*N*-dealkyl-); RT 4.1

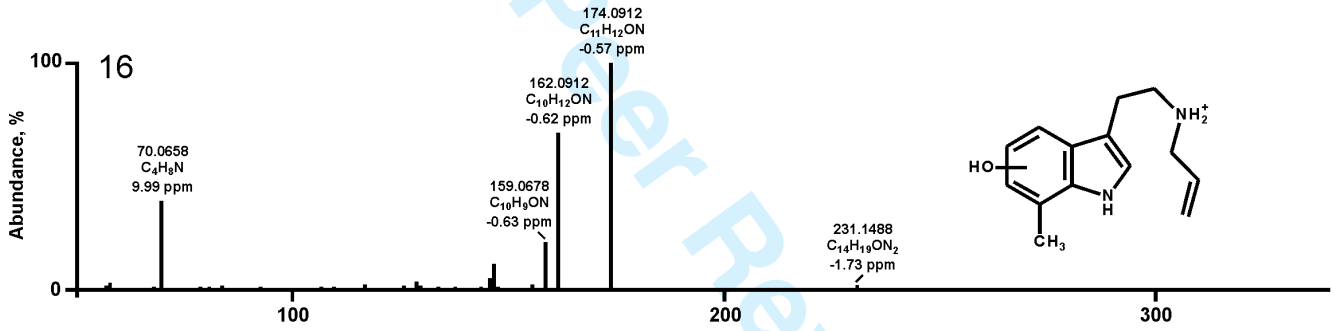

7-Me-DALT-M (*N*-dealkyl-HO-aryl-); RT 2.9

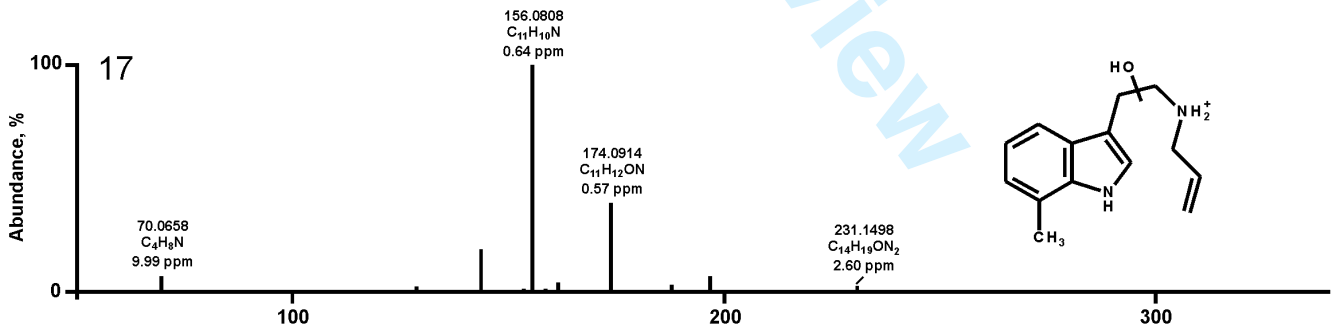

7-Me-DALT-M (*N*-dealkyl-HO-alkyl-); RT 3.3

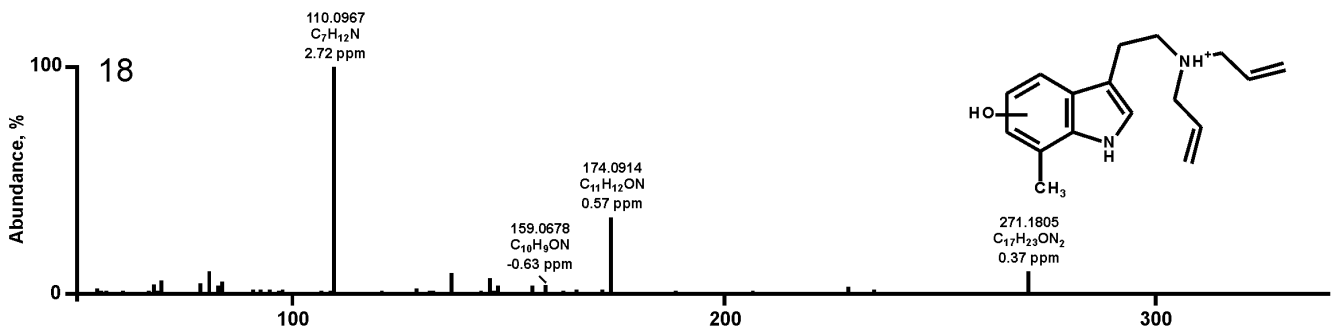

7-Me-DALT-M (HO-aryl-) isomer 1; RT 3.7

m/z

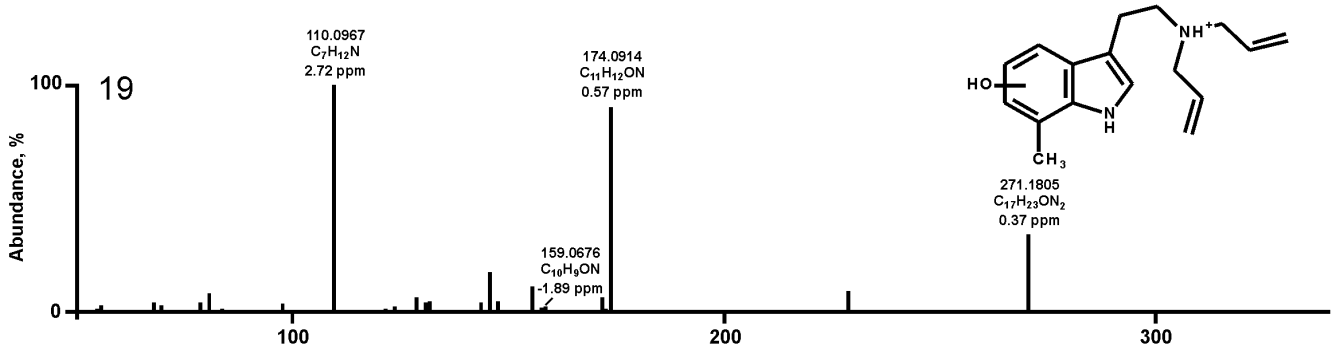

7-Me-DALT-M (HO-aryl-) isomer 2; RT 3.9

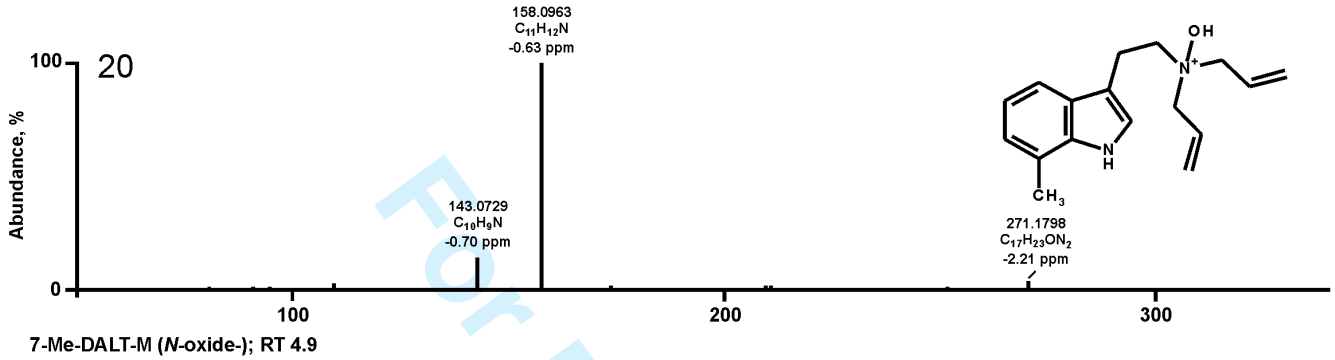

7-Me-DALT-M (*N*-oxide-); RT 4.9

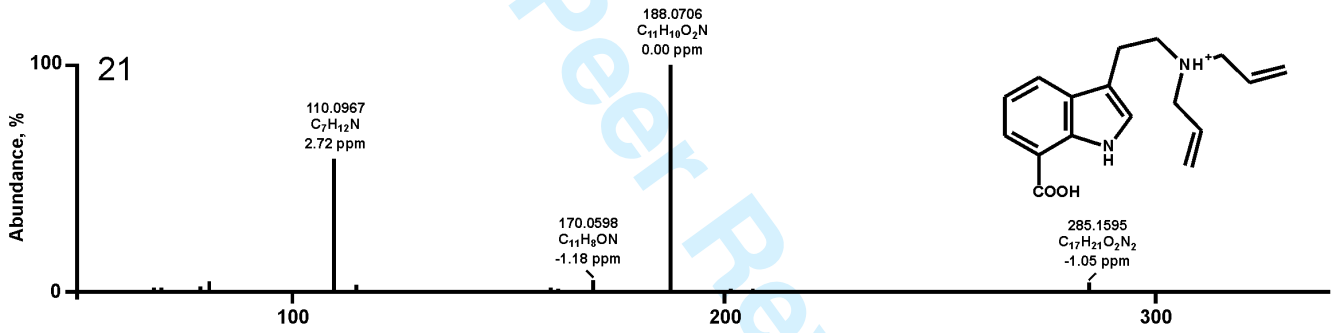

7-Me-DALT-M (carboxy-); RT 4.2

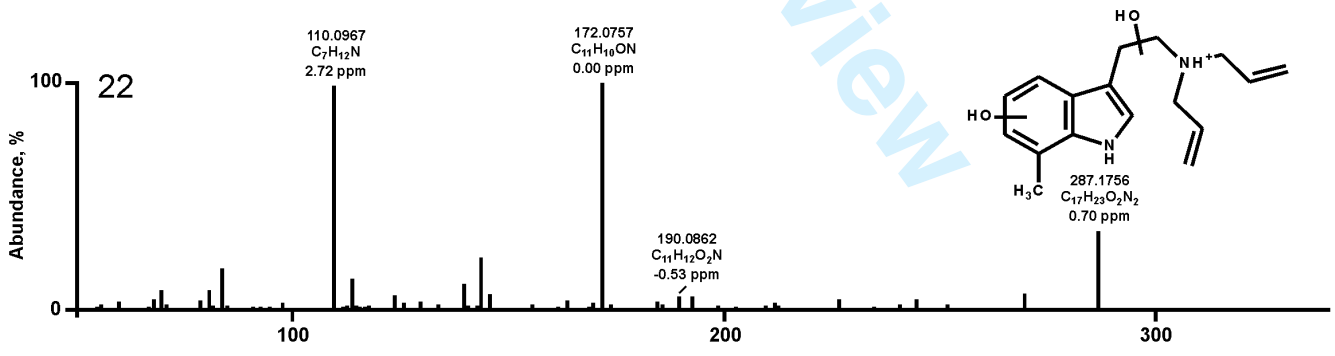

7-Me-DALT-M (HO-alkyl-HO-aryl-); RT 3.2

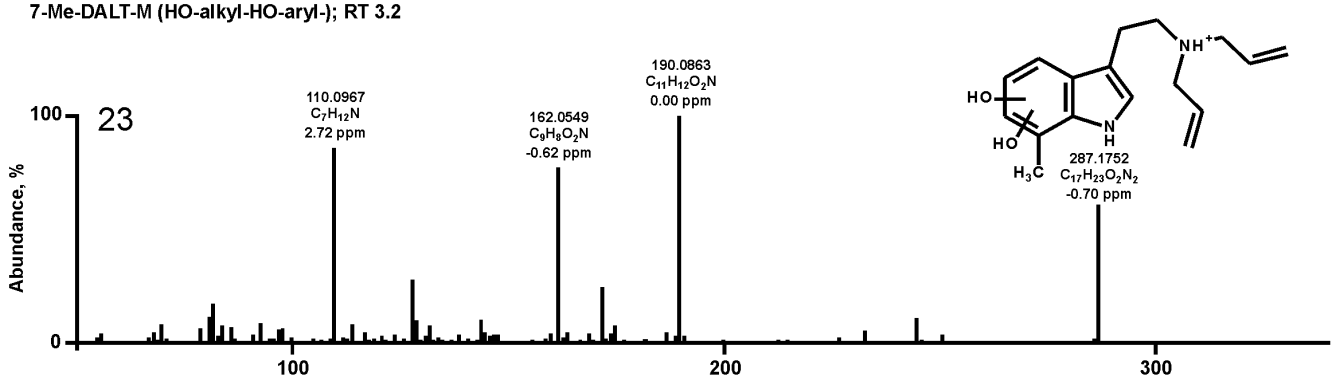

7-Me-DALT-M (di-HO-aryl-); RT 3.7

m/z

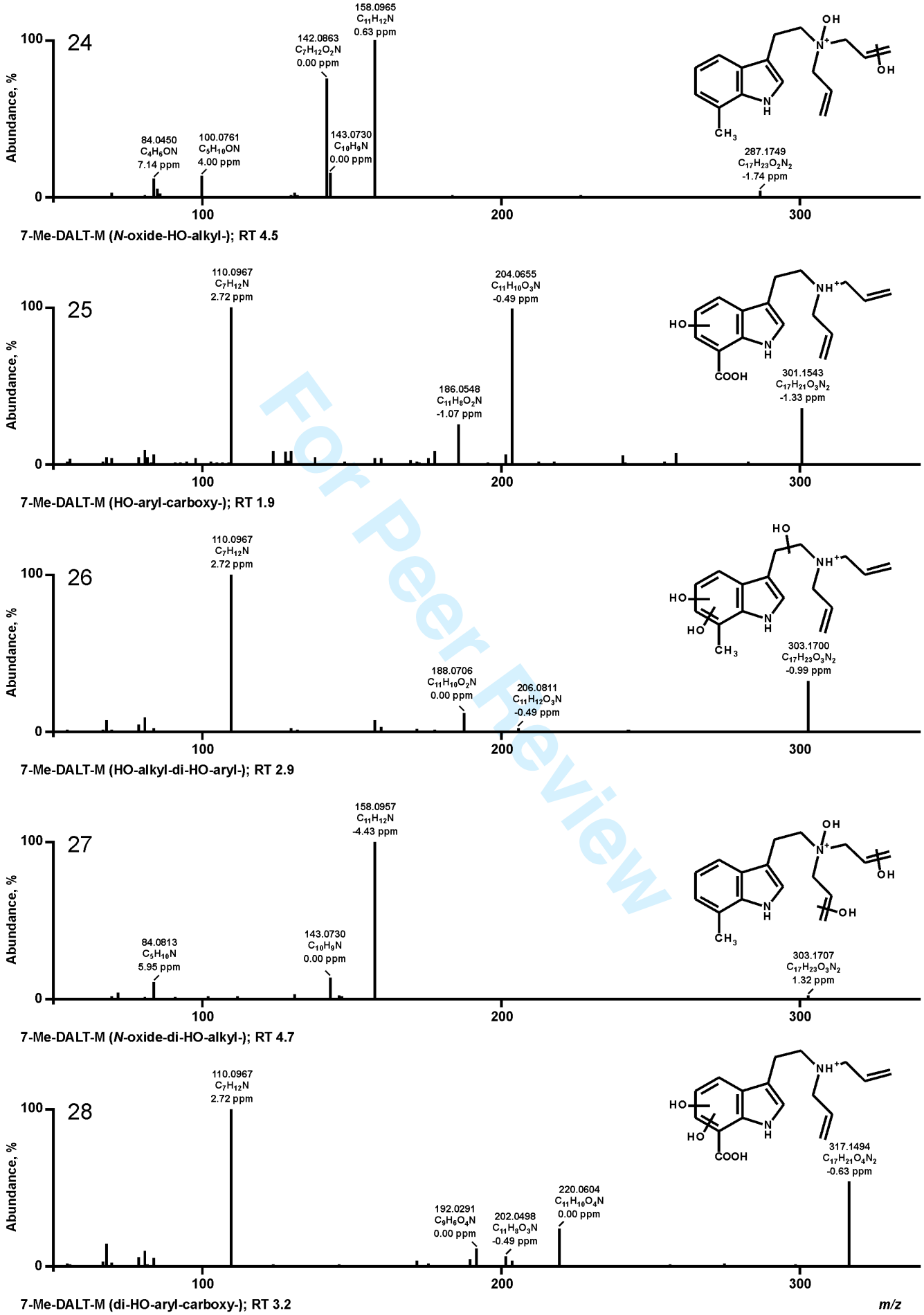

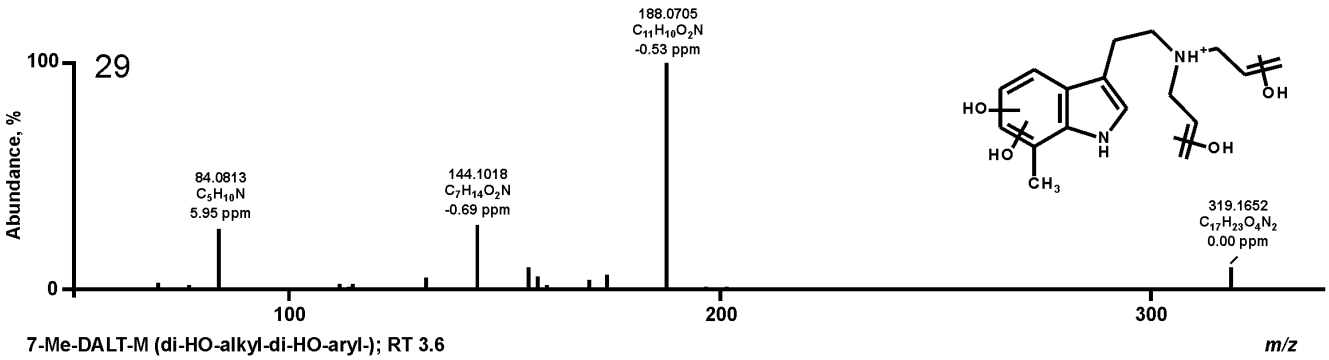

Fig. S2 LC-HR-MS/MS spectra of 7-Me-DALT and its phase I metabolites arranged according to their precursor values, proposed chemical structures, accurate masses, calculated elemental formulas, mass error values in parts per million (ppm), and retention times in minutes (min)

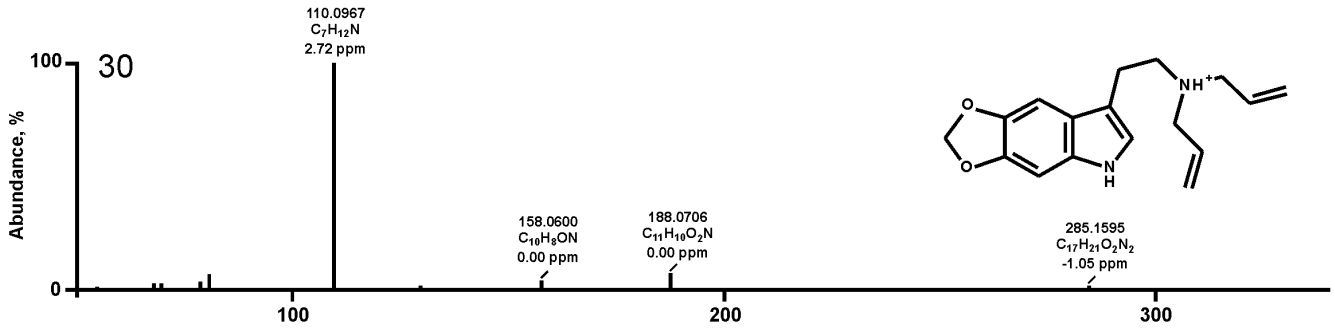

5,6-MD-DALT; RT 4.3

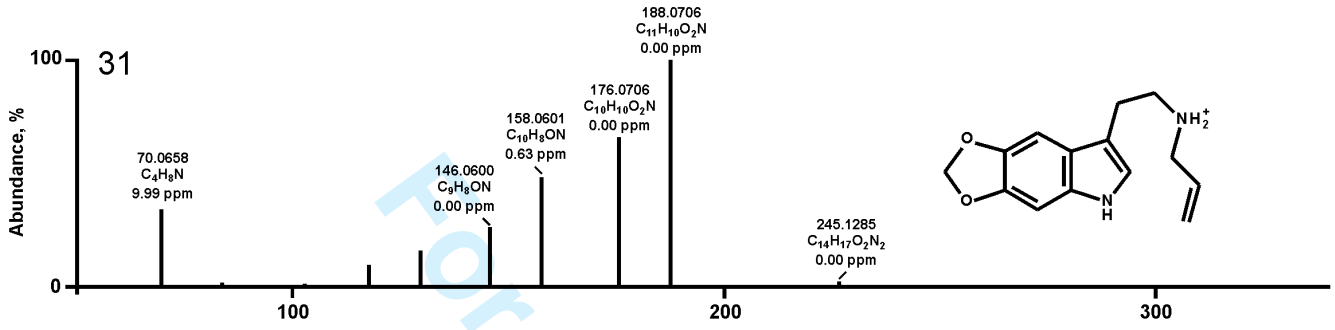

5,6-MD-DALT-M (*N*-dealkyl-); RT 3.7

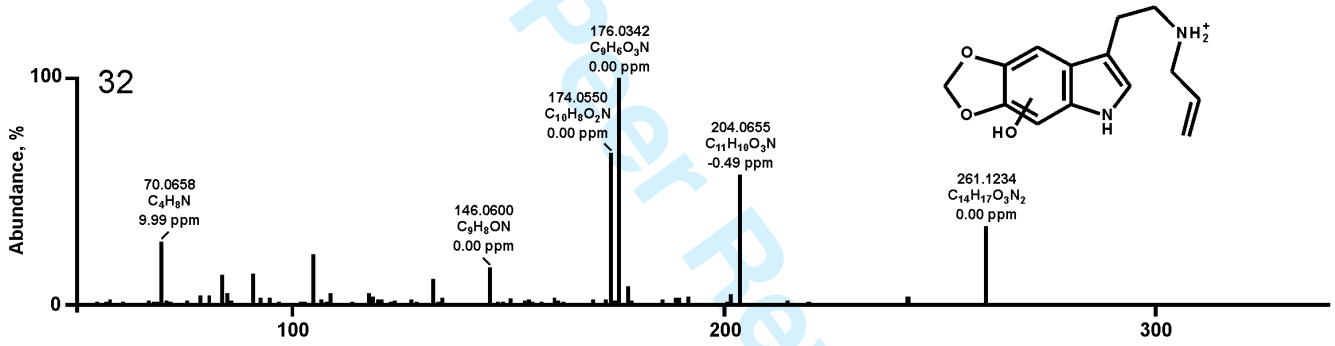

5,6-MD-DALT-M (*N*-dealkyl-HO-aryl-); RT 3.1

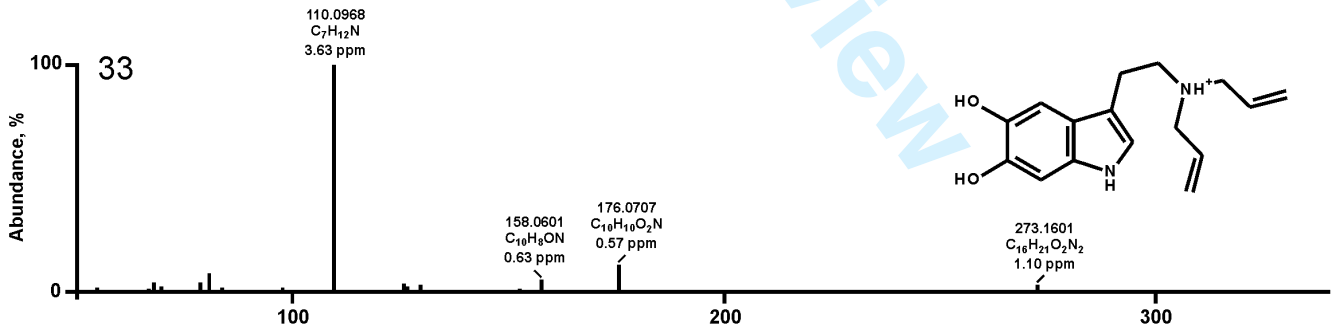

5,6-MD-DALT-M (demethyleneyl-); RT 3.3

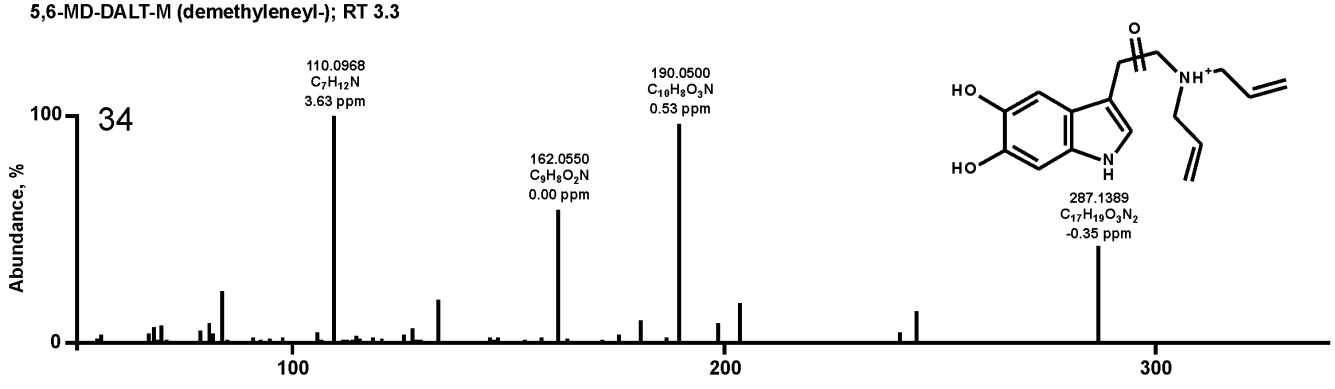

5,6-MD-DALT-M (demethyleneyl-oxo-); RT 3.9

m/z

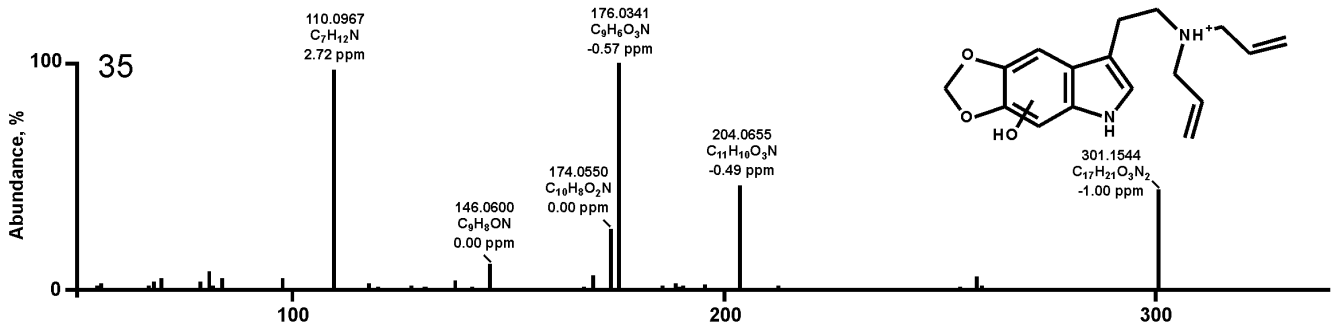

5,6-MD-DALT-M (HO-aryl-); RT 3.6

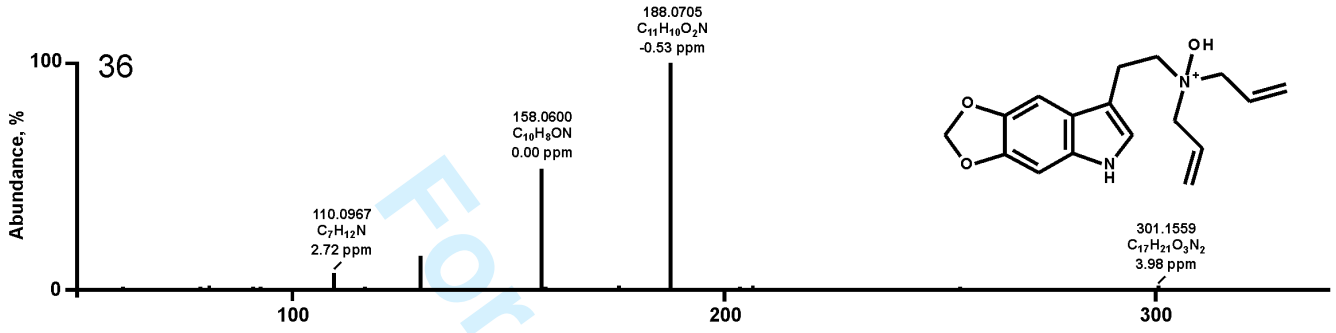

5,6-MD-DALT-M (*N*-oxide-); RT 4.5

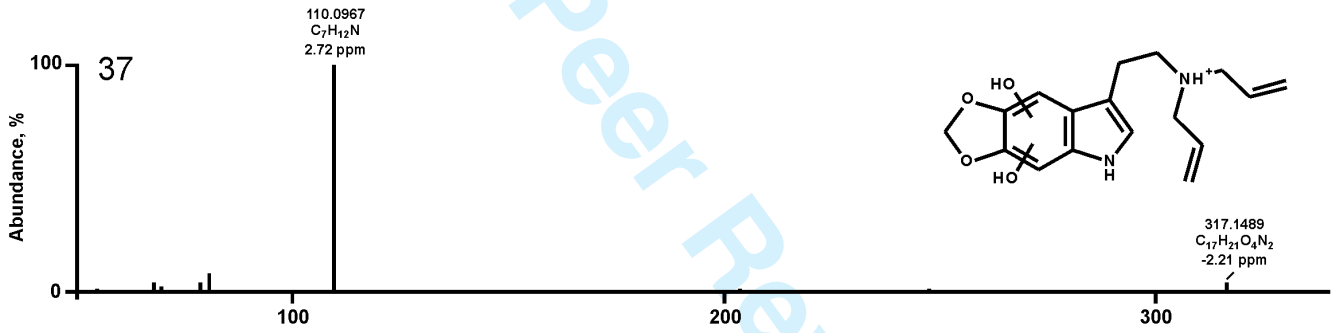

5,6-MD-DALT-M (di-HO-aryl-); RT 3.4

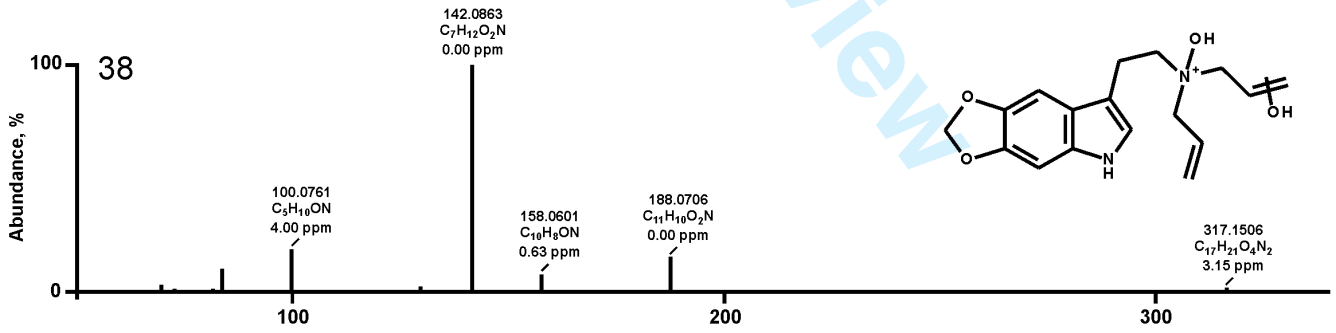

5,6-MD-DALT-M (*N*-oxide-HO-alkyl-); RT 4.0

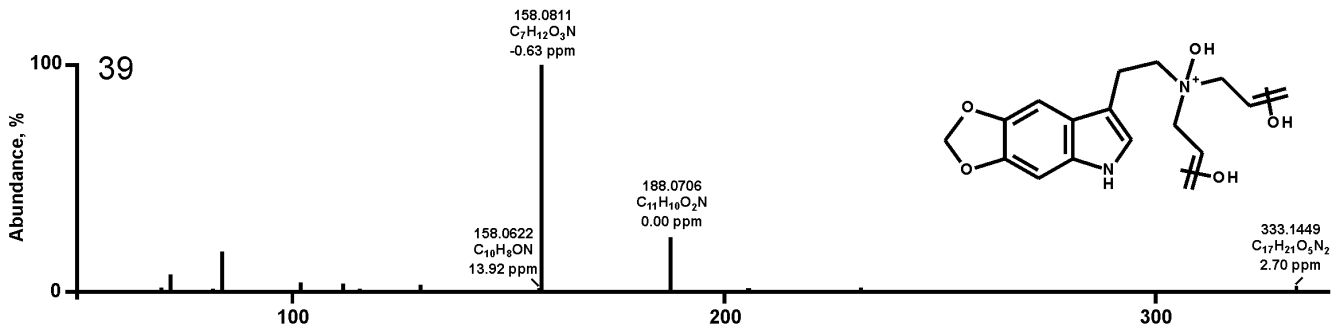

5,6-MD-DALT-M (*N*-oxide-di-HO-alkyl-); RT 4.2

Fig. S3 LC-HR-MS/MS spectra of 5,6-MD-DALT and its phase I metabolites arranged according to their precursor values, proposed chemical structures, accurate masses, calculated elemental formulas, mass error values in parts per million (ppm), and retention times in minutes (min)

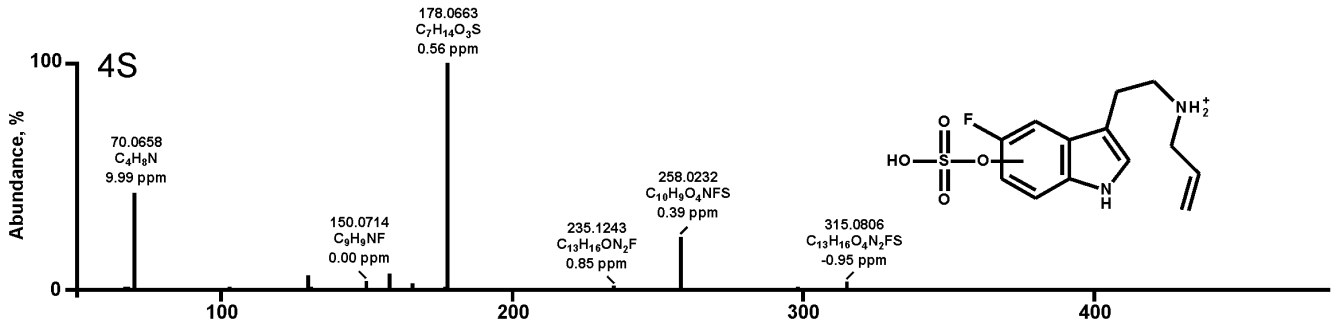

5-F-DALT-M (*N*-dealkyl-HO-aryl-sulfate) isomer 1; RT 3.5

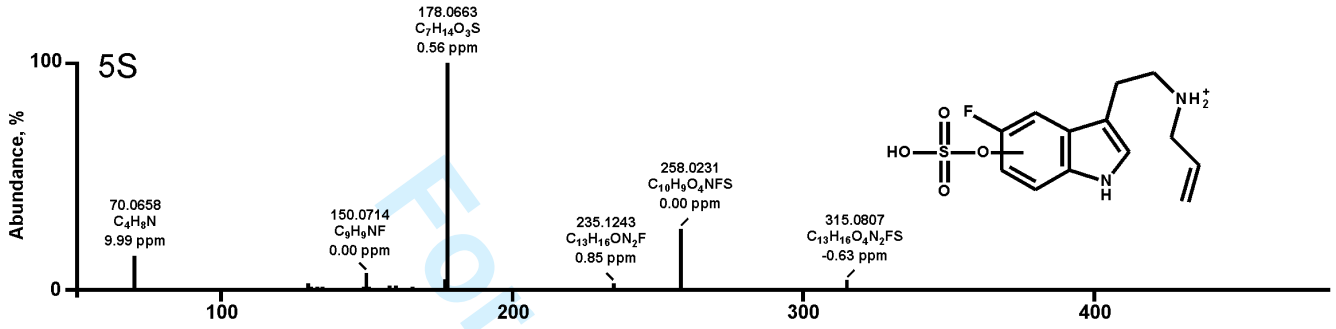

5-F-DALT-M (*N*-dealkyl-HO-aryl-sulfate) isomer 2; RT 4.1

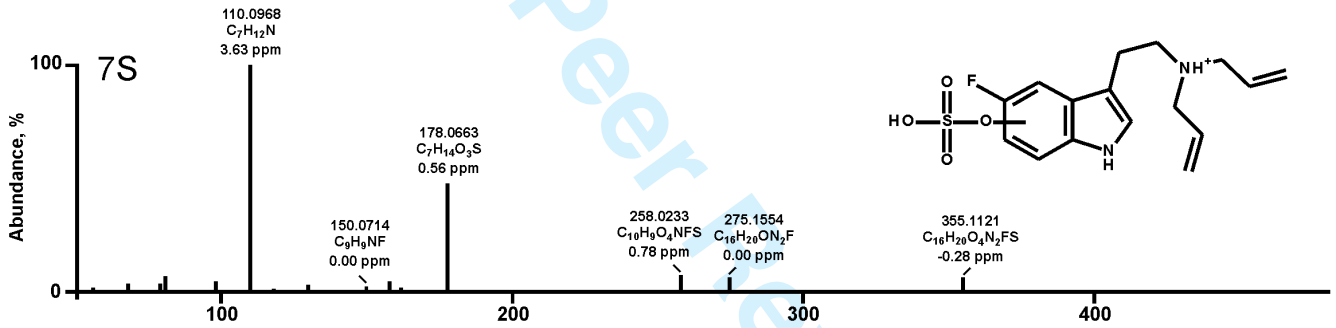

5-F-DALT-M (HO-aryl-sulfate); RT 4.1

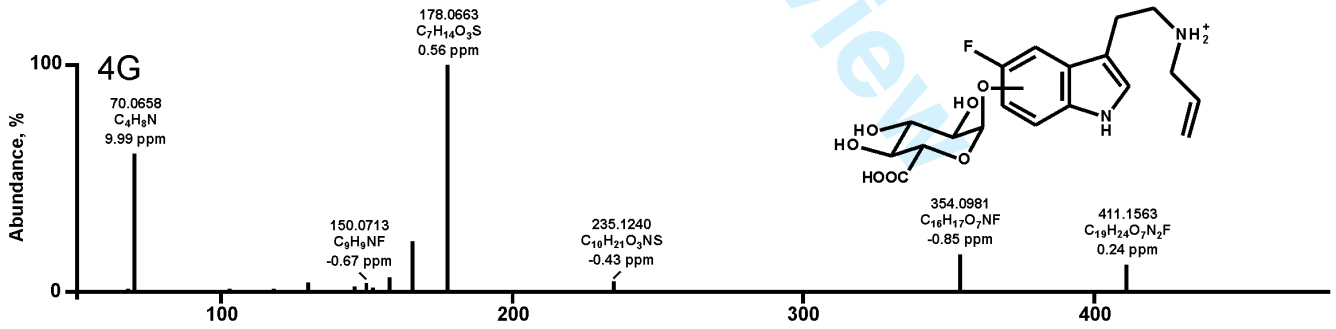

5-F-DALT-M (*N*-dealkyl-HO-aryl-glucuronide) isomer 1; RT 2.0

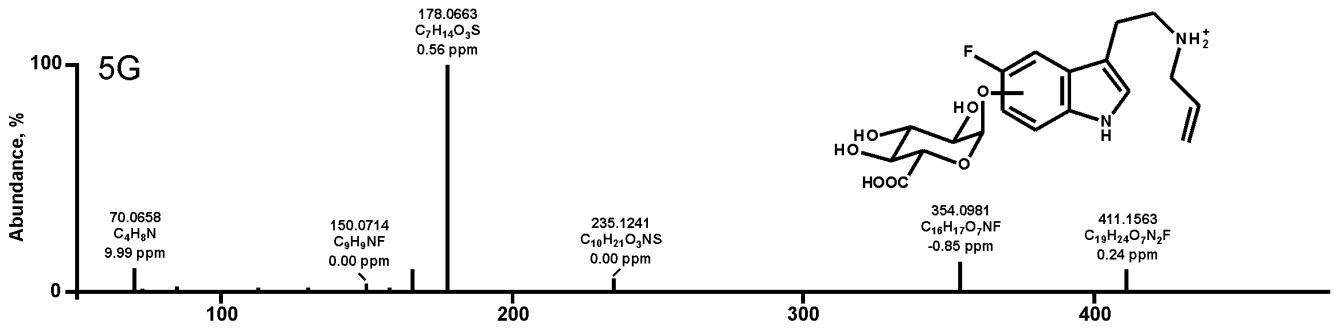

5-F-DALT-M (*N*-dealkyl-HO-aryl-glucuronide) isomer 2; RT 3.3

m/z

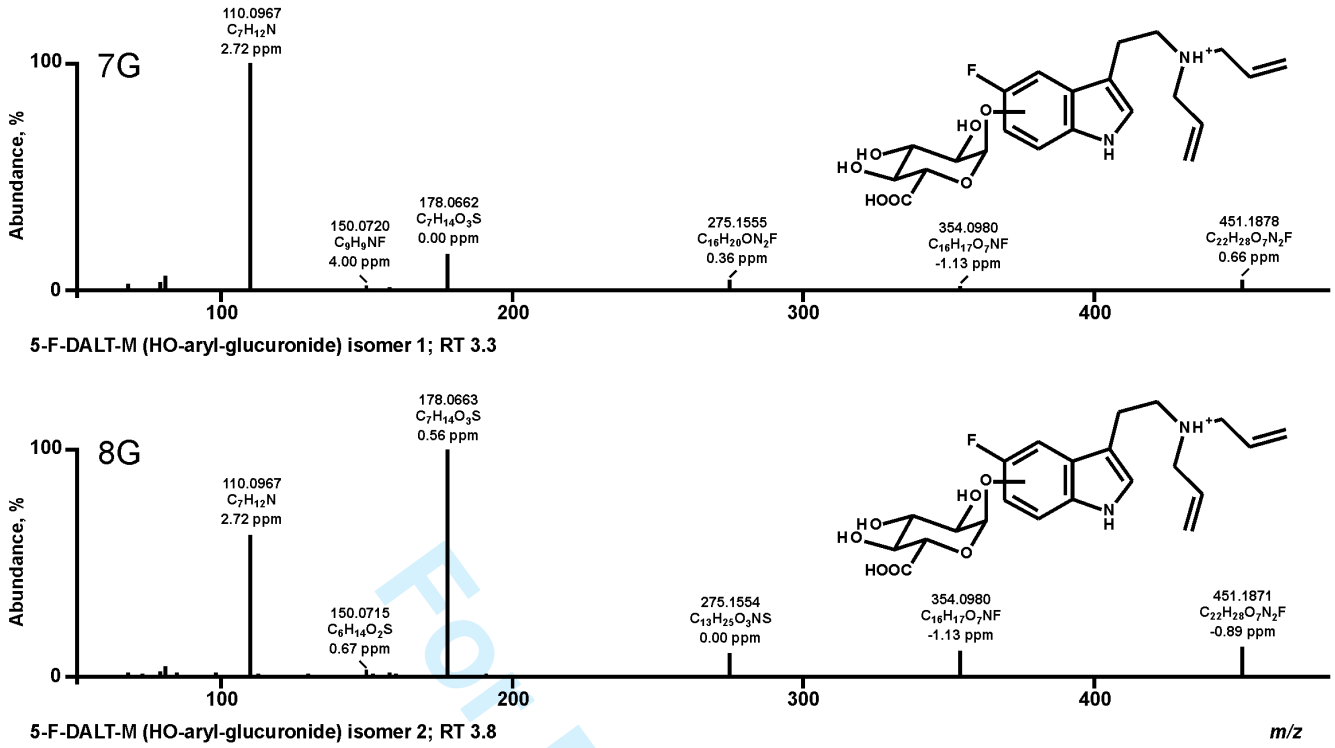

Fig. S4 LC-HR-MS/MS spectra of 5-F-DALT phase II metabolites arranged according to their precursor values, proposed chemical structures, accurate masses, calculated elemental formulas, mass error values in parts per million (ppm), and retention times in minutes (min)

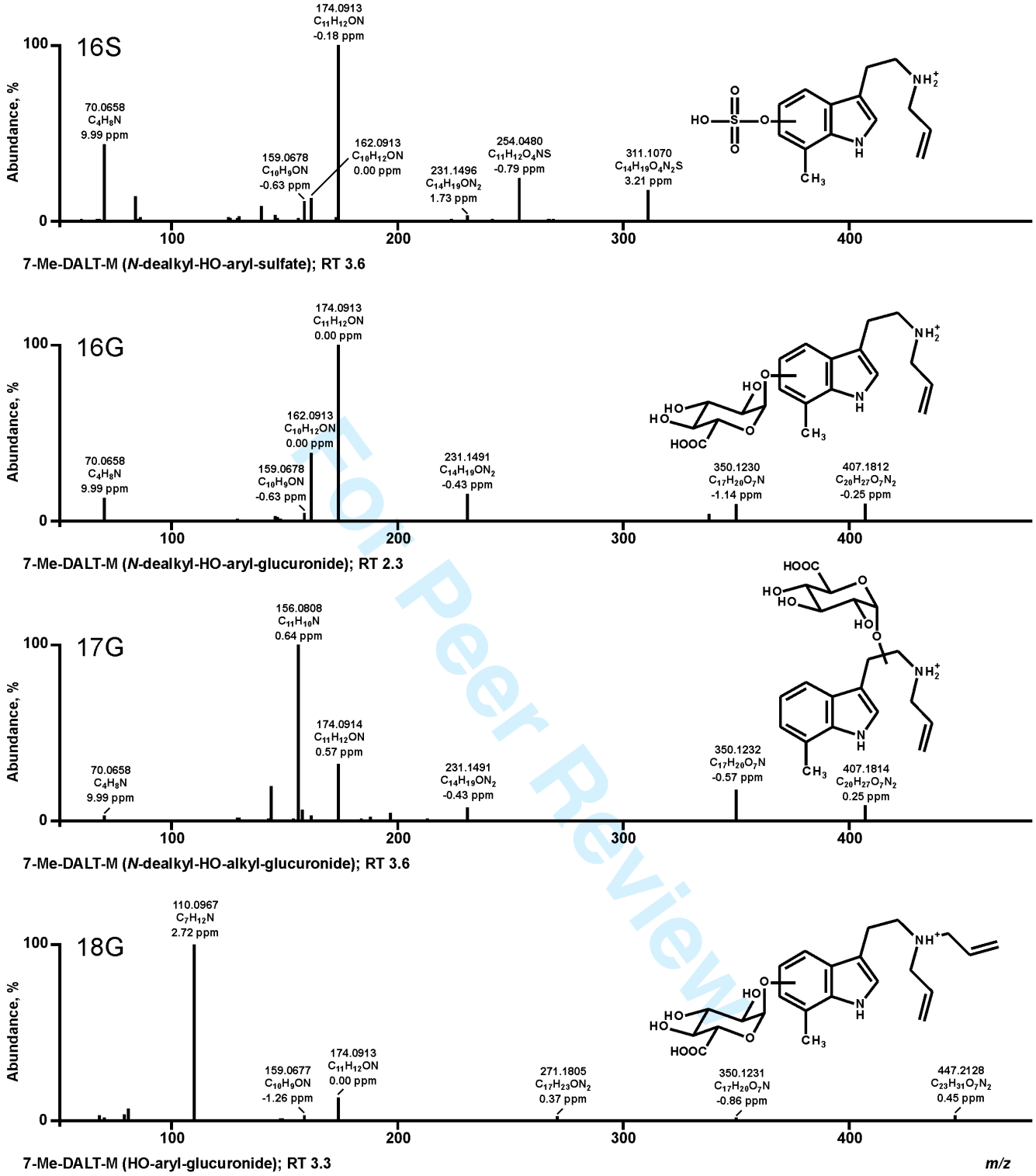

Fig. S5 LC-HR-MS/MS spectra of 7-Me-DALT phase II metabolites arranged according to their precursor values, proposed chemical structures, accurate masses, calculated elemental formulas, mass error values in parts per million (ppm), and retention times in minutes (min)

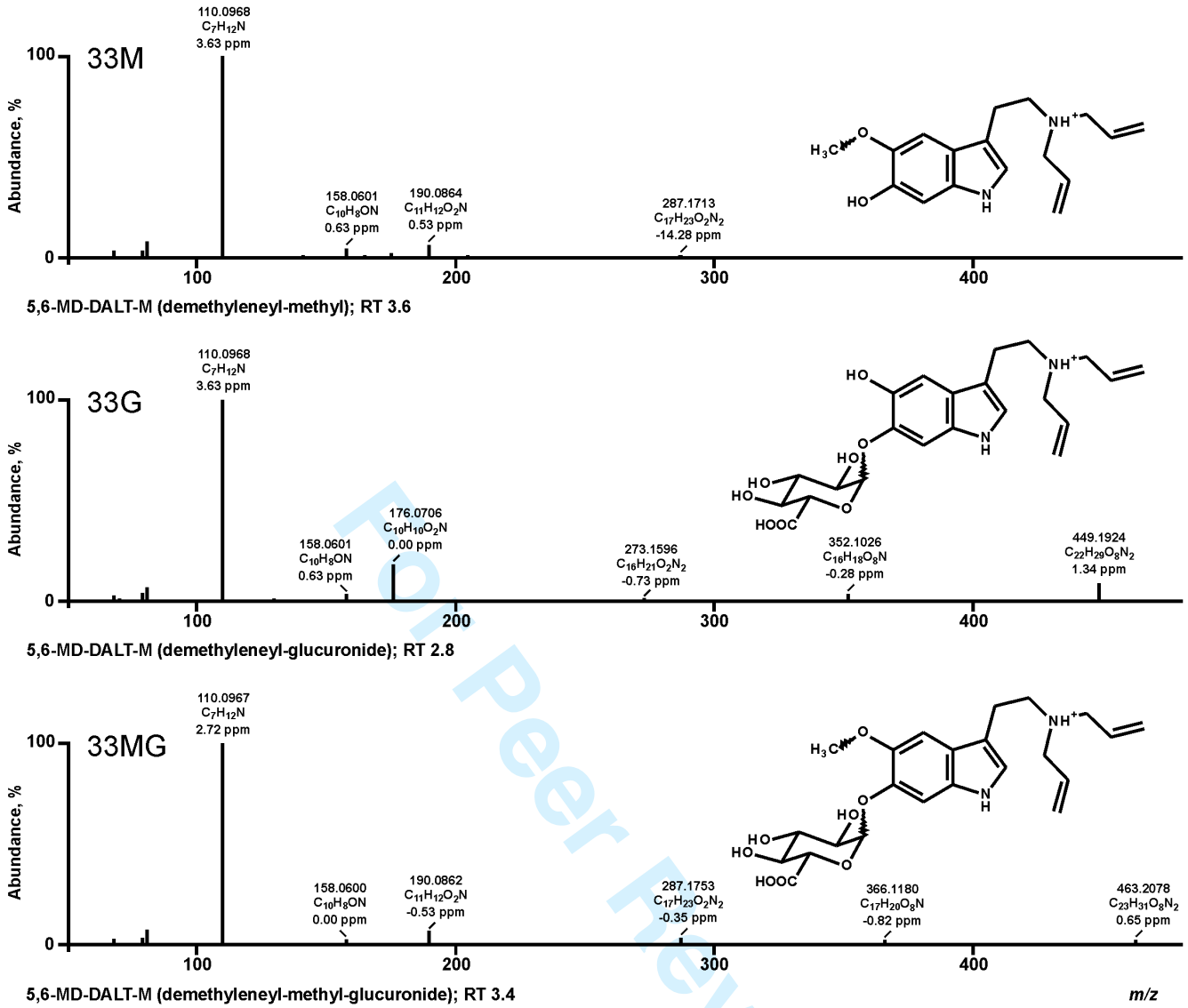

Fig. S6 LC-HR-MS/MS spectra of 5,6-MD-DALT phase II metabolites arranged according to their precursor values, proposed chemical structures, accurate masses, calculated elemental formulas, mass error values in parts per million (ppm), and retention times in minutes (min)